Observations of Cross-Shelf Flow Driven by Cross-Shelf Winds on the Inner Continental Shelf

MELANIE FEWINGS,* STEVEN J. LENTZ, AND JANET FREDERICKS

Woods Hole Oceanographic Institution, Woods Hole, Massachusetts

(Manuscript received 25 January 2008, in final form 11 April 2008)

ABSTRACT

Six-yr-long time series of winds, waves, and water velocity from a cabled coastal observatory in 12 m of water reveal the separate dependence of the cross-shelf velocity profile on cross-shelf and along-shelf winds, waves, and tides. During small waves, cross-shelf wind is the dominant mechanism driving the cross-shelf circulation after tides and tidal residual motions are removed. The along-shelf wind does not drive a substantial cross-shelf circulation. During offshore winds, the cross-shelf circulation is offshore in the upper water column and onshore in the lower water column, with roughly equal and opposite volume transports in the surface and bottom layers. During onshore winds, the circulation is nearly the reverse. The observed profiles and cross-shelf transport in the surface layer during winter agree with a simple two-dimensional unstratified model of cross-shelf wind stress forcing. The cross-shelf velocity profile is more vertically sheared and the surface layer transport is stronger in summer than in winter for a given offshore wind stress.

During large waves, the cross-shelf circulation is no longer roughly symmetric in the wind direction. For onshore winds, the cross-shelf velocity profile is nearly vertically uniform, because the wind- and wave-driven shears cancel; for offshore winds, the profile is strongly vertically sheared because the wind- and wave-driven shears have the same sign. The Lagrangian velocity profile in winter is similar to the part of the Eulerian velocity profile due to cross-shelf wind stress alone, because the contribution of Stokes drift to the Lagrangian velocity approximately cancels the contribution of waves to the Eulerian velocity.

1. Introduction

On continental shelves, cross-shelf circulations influence the water column density structure and the distributions of heat, salt, phytoplankton, nutrients, and pollutants. Cross-shelf exchange is an important mechanism for supplying nutrients to continental shelf ecosystems, which are some of the most productive on earth (Falkowski et al. 1998). On the inner continental shelf in particular, cross-shelf exchange is thought to influence the ecosystem by transporting heat, nutrients, and larvae between the surfzone and midshelf (e.g., Roughgarden et al. 1988; Austin 1999).

The inner shelf is a complex region offshore of the surfzone, where the surface and bottom boundary layers interact (e.g., Lentz 1994, 1995). The location of the boundary between the inner shelf and the midshelf changes with time, depending on the thicknesses of the surface and bottom boundary layers, which determine the water depth where the boundary layers overlap. As a result of the overlapping boundary layers, the inner shelf exhibits a divergence in the cross-shelf transport driven by along-shelf winds, which leads to coastal upwelling and downwelling (Ekman 1905).

The mechanisms that drive cross-shelf flow over the inner shelf are not well understood. In the middle and outer regions of the shelf, along-shelf winds drive coastal upwelling and downwelling circulations that transport material and heat in the cross-shelf direction (e.g., Ekman 1905; Sverdrup 1938; Smith 1981). Observations on the North Carolina (Lentz 2001), Oregon (Kirincich et al. 2005), and California (Cudaback et al. 2005) continental shelves and numerical model studies (e.g., Austin and Lentz 2002; Tilburg 2003) show, however, that the along-shelf wind is not very effective at driving cross-shelf flow on the inner shelf. Along-shelf

* Current affiliation: Marine Science Institute, University of California, Santa Barbara, Santa Barbara, California.

Corresponding author address: Melanie R. Fewings, Marine Science Institute, University of California, Santa Barbara, Santa Barbara, CA 93106-6150.
E-mail: melanie@icess.ucsb.edu

DOI: 10.1175/2008JPO3990.1

© 2008 American Meteorological Society

Unauthenticated | Downloaded 10/26/25 08:20 PM UTC

variations in topography and along-shelf currents are other proposed mechanisms for cross-shelf exchange flows on the inner shelf (Austin and Lentz 2002).

Here, we examine a different mechanism for driving cross-shelf exchange on the inner shelf: cross-shelf wind. Cross-shelf wind stresses are usually assumed ineffective at driving shelf circulations (e.g., Csanady 1978; Allen 1980; Brink 1998). Over middle and outer continental shelves, the cross-shelf momentum balance is typically geostrophic on subtidal time scales: the cross-shelf pressure gradient force balances the Coriolis force due to the along-shelf flow (Brown et al. 1985; Thompson and Pugh 1986; Brown et al. 1987; Noble and Butman 1983; Lee et al. 1984, 1989; Lentz et al. 1999; Shearman and Lentz 2003; Liu and Weisberg 2005). Therefore, the cross-shelf wind stress is relatively unimportant in the steady depth-average momentum balance at midshelf. The mountain-gap winds in the gulfs of Tehuantepec and Papagayo are exceptions, where the wind stress curl due to spatial variations in a strong cross-shelf wind forces a substantial cross-shelf circulation, even outside the inner shelf (McCreary et al. 1989). In contrast, our focus here is on spatially uniform wind stress.

The ratio R of the cross-shelf wind stress to the Coriolis force due to along-shelf flow, $R = \tau_s^x/(\rho_0 f h v_{da})$, where τ_s^x is cross-shelf wind stress, ρ_0 is water density, f is the Coriolis parameter, h is water depth, and v_{da} is depth-average along-shelf current, suggests that the cross-shelf wind stress is an important term in the momentum balance, where h is small or v_{da} is weak. We estimate R for a number of sites along the Middle Atlantic Bight continental shelf by comparing the standard deviations of τ_s^x and $\rho_0 f h v_{da}$ on subtidal time scales (Fig. 1). [Note that R goes roughly as h^{-1}, and R is plotted against h in Fig. 1. We do not use Fig. 1 to argue for a relation between h^{-1} and h but to illustrate the water depths h at which $R \sim O(1)$]. The estimates in Fig. 1 suggest that the cross-shelf wind stress is 30% or more of the Coriolis term in water depths less than 25 m, at midlatitudes on the east coast of the United States. At the Martha's Vineyard Coastal Observatory (MVCO), the ratio is 0.65, indicating that the cross-shelf wind stress is an important forcing mechanism at this site. The large spread in R values in shallow water is due to smaller variability in τ_s^x and larger variability in v_{da} at sites farther to the south in the Middle Atlantic Bight (sites south of latitude 38°N are indicated by open symbols in Fig. 1). Momentum balances calculated from observations in 10–16-m water depth in the South Atlantic Bight (Blanton 1981; Lee et al. 1989), 8-m depth in the Middle Atlantic Bight (Lentz et al. 1999), and 15-m depth on the West Florida shelf (Liu and Weisberg 2005) also indicate that cross-shelf wind stress is an important term in shallow water.

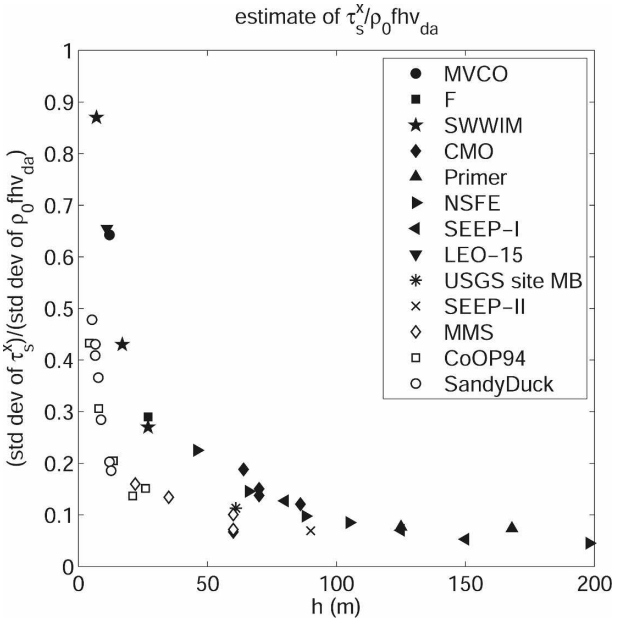

FIG. 1. Size of cross-shelf wind stress, relative to Coriolis term in depth-integrated cross-shelf momentum balance, for several sites along the U.S. east coast. The wind stress and depth-average flow for each site are calculated in the same way as for MVCO. The cross-shelf wind stress is an important forcing term (indicating the cross-shelf momentum balance is not geostrophic) in water shallower than about 25 m. The sites are MVCO; CBLAST F (Hutto et al. 2005); SWWIM (Lentz et al. 2008); CMO (Shearman and Lentz 2003); Shelf-break Primer (Fratantoni and Pickart 2003); NSFE (Beardsley et al. 1985); SEEP-I (Walsh et al. 1988); LEO-15 (Schofield et al. 2002); SEEP-II (Biscaye et al. 1994); USGS site MB (http://stellwagen.er.usgs.gov/mab_sed.html); CoOP94 (Lentz et al. 1999); MMS (Berger et al. 1994); and SandyDuck (http://www.frf.usace.army.mil/SandyDuck/SandyDuck.stm).

The cross-shelf wind stress, in addition to being important in the momentum balance, may drive a substantial cross-shelf circulation. Analytical theories (Ekman 1905; Garvine 1971) and an idealized numerical modeling study (Tilburg 2003) suggest that cross-shelf winds could drive significant cross-shelf circulations where the water is shallow enough that the entire water column is within the overlapping top and bottom boundary layers (i.e., on the inner shelf). Numerical modeling studies of the West Florida shelf suggest that the cross-shelf wind stress plays an important role in driving along-shelf and cross-shelf currents over that inner shelf (Li and Weisberg 1999b,a). In the Santa Barbara Channel in California, strong offshore wind stresses south of a mountain pass are significantly correlated with a two-layer cross-shelf circulation over the inner shelf, with surface-intensified offshore flow in the upper water column and onshore flow in the lower water column (Cudaback et

Unauthenticated | Downloaded 10/26/25 08:20 PM UTC

al. 2005). Nevertheless, there has been no observational study that examines the dependence of the cross-shelf velocity profile in the inner shelf on the strength of the cross-shelf wind forcing.

It has previously been difficult to separate the influences of waves, cross-shelf wind, and along-shelf wind in observational studies because all three types of forcing are usually correlated. With a nearly 6-yr-long time series of wind, wave, and velocity data, however, we are able for the first time to look at the structure of the cross-shelf flow during times when only one of the three types of forcing was strong. The cross-shelf flow circulation at this site is driven by cross-shelf winds, surface gravity waves (Lentz et al. 2008), and tides, not by along-shelf winds. The dependence of the cross-shelf flow on wave forcing alone is discussed in Lentz et al. (2008). We briefly discuss the tidally driven residual circulation here, but tidal effects are beyond the scope of this paper. Here, we examine the response of the cross-shelf flow to cross-shelf wind stress alone, along-shelf wind stress alone, and combined waves and cross-shelf wind stress. We demonstrate that cross-shelf winds are more effective than along-shelf winds at driving cross-shelf exchange flow at this inner shelf site. We also show that the response to combined wave and cross-shelf wind stress forcing is roughly the sum of the separate responses to wave forcing and cross-shelf wind stress forcing, at least in winter.

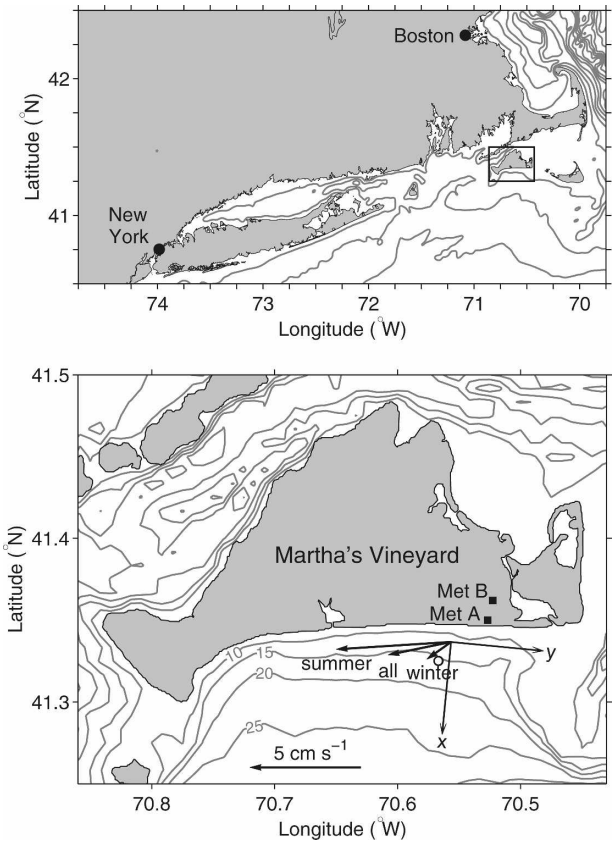

FIG. 2. (top) Location of study area (outlined square). (bottom) Detailed map of MVCO study area, with time-mean depth-average flow vectors for all times, winter, and summer (for all wave conditions). The along-shelf–cross-shelf coordinate system is based on the principal axis direction of the depth-average subtidal flow. The MVCO ADCP is located at the origin of the coordinate system. Open circle indicates ASIT. Mean flow during small waves is nearly along the $-y$ axis. Isobaths are labeled in meters.

2. Data and methods

a. Martha's Vineyard Coastal Observatory

We use time series of water velocity profiles, wave, and meteorological data that extend over 6 yr from the cabled MVCO. An underwater node for this observatory is located 1.5 km off the south shore of Martha's Vineyard, Massachusetts, on the northeastern United States continental shelf at 41°20.2′N, 70°33.39′W, in 12 m of water, well outside the surfzone (Fig. 2). The long time series used here are from a bottom-mounted acoustic Doppler current profiler (ADCP) and temperature and pressure sensors, all located at the underwater node and connected to a shore laboratory by underwater power and fiber-optic data transmission cables. Meteorological data are from two masts on Martha's Vineyard (Met A at 41°21.0′N, 70°31.6'W, which is 2.5 km east and 1.5 km north of the underwater node, and Met B at 41°21.72′N, 70°31.35′W). Wind stress was calculated from the Smith (1988) bulk formula, using wind velocity measured 12.5 m above sea level. The wind stress at Met B was linearly adjusted to be representative of wind stress nearer the shore at Met A (see appendix A of Fewings 2007). Using the adjusted winds does not qualitatively change the results, compared to using only the Met A winds.

The data cover the period from 19 June 2001 to 10 May 2007. More data are available during winter than summer. The instrument sampling frequencies are all between 2 Hz and 1 cycle min^{-1}. The data are archived by the Woods Hole Oceanographic Institution, and time series of 20-min-average water velocity, meteorological data, and spectrally resolved wave data are available online (http://www.whoi.edu/mvco). Detailed information about the instruments is also available at this site.

There are four periods of at least one month with no available data: September through November 2001, June through July 2002, May through August 2004, and August 2005. In addition, we discarded the velocity and wave data during several periods when the signal cor-

Unauthenticated | Downloaded 10/26/25 08:20 PM UTC

relation from the ADCP was low: 7 February to 17 April 2002, 22 February to 4 April 2004, 8–19 April 2005, 2 February to 7 March 2006, and 25 February to 24 April 2007. We linearly interpolated across all gaps shorter than 12 h.

b. Coordinate system

We define the along-shelf direction as the major principal axis direction of the depth-average subtidal flow (defined in section 2.5) when waves are small (significant wave height $H_{sig} \lesssim 0.75$ m), as in Lentz et al. (2008). The major principal axis direction is oriented 5.5° clockwise from east, roughly parallel to the local isobaths (Fig. 2).

We use a coordinate system with x positive offshore, y positive along-shelf eastward, and z positive upward, where $z = 0$ is the mean sea surface height over the deployment. The horizontal component of the water velocity in this coordinate system is $\mathbf{u} = (u, v)$. The wind stress is $\boldsymbol{\tau_s} = (\tau_s^x, \tau_s^y)$.

c. Water velocity

The MVCO ADCP is a 1200-kHz RDI Workhorse Monitor deployed in a bottom-mounted, upward-looking configuration with 0.5-m bins from $z_{bot} = -9.5$ to $z_{top} = -2.0$ m. The top good bin is based on the bin-to-bin shear and the signal correlation from the ADCP.

To calculate depth-average velocities (below the wave troughs), we assumed the velocity to be constant from the lowest ADCP bin to the bottom ($z = -12$ m) and from the top good ADCP bin to the mean water surface. The results presented here do not change significantly if we instead use linear extrapolation to the surface and/or bottom.

d. Waves

The significant wave height H_{sig}, dominant wave period T_w, wave direction θ_w, and wave phase speed c are calculated from the ADCP velocity measurements as described on the MVCO Web site. The predicted onshore volume transport due to the dominant waves, Q_w, is (Longuet-Higgins 1953)

$$Q_w = \frac{gH_{sig}^2}{16c}\cos\theta_w, \tag{1}$$

where g is the acceleration due to gravity and θ_w is the direction the waves are going, measured counterclockwise from the positive x axis ($\theta_w = 180°$ indicates waves propagating directly onshore). Note that Q_w depends on the wave period T_w through the phase speed $c(T_w)$. This volume transport Q_w takes place above the wave troughs in an Eulerian reference frame (Fig. 3, left). We use $F_w \equiv H_{sig}^2 \cos\theta_w$ to indicate the strength of the wave forcing. For a typical wave propagating directly onshore at MVCO, with period $T_w = 5.5$ s and significant wave height $H_{sig} = 1$ m, $F_w = -1$ m^2 and $Q_w = -0.08$ m^2 s^{-1}.

If the circulation is along-shelf uniform, there is a predicted offshore return flow (undertow) with a volume transport equal to $-Q_w$. The observed offshore volume transport does tend to equal $-Q_w$ (Lentz et al. 2008). Also see Lentz et al. (2008) for discussion of the vertical structure of the undertow at this site.

e. Removing tides

The tidal velocities at MVCO are dominated by the M_2 tide (the lunar semidiurnal tide, with period 12.42 h) and are relatively large (Shearman and Lentz 2004). Near the surface on the 12-m isobath, the tidal velocity reaches 25 cm s^{-1} for the M_2 tide and over 35 cm s^{-1} for the full tide; the depth-average tidal velocities reach 30 cm s^{-1}. These tidal velocities are elliptical (eccentricity $\varepsilon = 0.1$) and oriented nearly along shelf (the major axis orientation is 1.5° counterclockwise from due east for the M_2 tide). The tidal velocities in the MVCO area are dominated by clockwise rotation, and the sea level elevation for the M_2 tide is $O(40$ cm) near MVCO and increases to the west (Shearman and Lentz 2004). The tidal components other than M_2 with major axis amplitude at least 2 cm s^{-1} at any ADCP bin at the MVCO Node are the K_1, N_2, and S_2 tides. The tide [as determined by T_TIDE (Pawlowicz et al. 2002)] contributes 79% (74%) of the variance in the along- (cross-) shelf depth-average- velocity 20-min time series.

Because we are interested here in the nontidal component of the velocity, we low-pass filtered the wind, wave, and detided water velocity time series with a 24-h cutoff (diurnal tides and sea breezes are weak in this area). For details, see Fewings (2007). We refer to the filtered velocity as the subtidal flow.

f. Surface layer transport

To calculate the wind-driven cross-shelf transport in the surface layer, we separate the cross-shelf flow $u(z, t)$ into a depth-average part $u_{da}(t)$ and a depth-varying part $\tilde{u}(z, t)$:

$$\tilde{u}(z, t) = u(z, t) - u_{da}(t), \tag{2}$$

where

$$u_{da}(t) = \frac{1}{h}\int_{-h}^{0} u(z, t)\, dz. \tag{3}$$

Unauthenticated | Downloaded 10/26/25 08:20 PM UTC

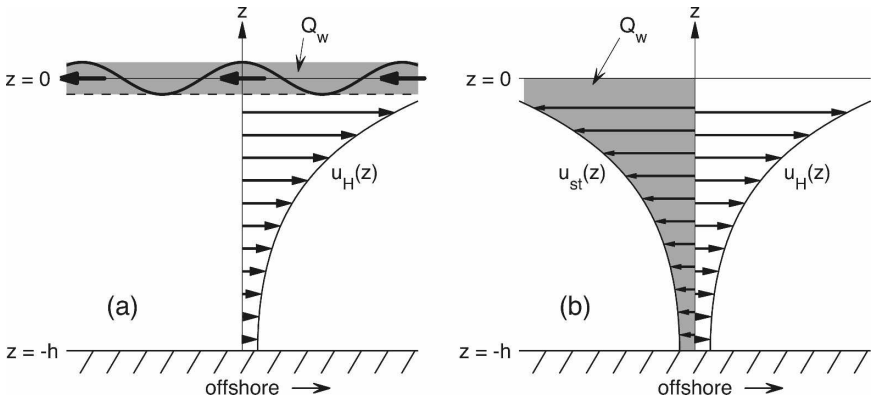

FIG. 3. (a) Two-dimensional wave-driven circulation in an Eulerian reference frame (fixed in space). Above the wave troughs (above dashed line), there is a net wave-averaged onshore volume transport Q_w (indicated by the gray shaded area and thick arrows). This is because in an Eulerian frame above the wave troughs there is either no water or water that has an onshore wave-averaged velocity. The wavy line indicates an instantaneous view of the sea surface. Because the circulation is two-dimensional, there must be a compensating Eulerian offshore volume transport $-Q_w$ below the wave troughs, which we refer to as undertow. Here, the undertow is shown with the vertical distribution u_H predicted by Hasselmann (1970). (b) Two-dimensional wave-driven circulation in a Lagrangian (particle following) reference frame. There is an onshore particle velocity, the Stokes drift $u_{st}(z)$, at all depths. The onshore volume transport due to this water parcel motion is Q_w (indicated by the gray shaded area). There is also an offshore particle velocity at all depths due to the undertow. If the undertow is distributed as $u_H(z) = -u_{st}$, it exactly cancels the Stokes drift and the net particle motion and net volume transport are both zero. If the undertow is not distributed as u_H, the net particle motion will not be zero, but the net volume transport will still be zero as long as the vertical integral of the undertow is equal to $-Q_w$.

We define the cross-shelf surface layer transport U_s as

$$U_s(t) = \int_{z_{\text{cross}}}^{0} \tilde{u}(z, t)\, dz, \tag{4}$$

where z_{cross} is the depth of the first zero crossing of $\tilde{u}(z,t)$. Here, U_s is an Eulerian cross-shelf volume transport per unit along-shelf distance. The total cross-shelf velocity $u(z, t)$ is driven by a combination of cross-shelf and along-shelf winds, waves, tides, and any other forcing that is present (e.g., pressure gradients due to topographic variations). We are interested only in the wind-driven part of the depth-dependent cross-shelf transport. We subtract the depth-average flow from $u(z, t)$ to calculate U_s following the approach of previous observational studies (Lentz 2001; Kirincich et al. 2005).

g. Bin averaging

We take advantage of the large number of synoptic wind and wave forcing events in the MVCO time series to separate those events into cases in which only the cross-shelf wind or the along-shelf wind forcing is strong and the other wind component and the waves are weak (see sections 4a,b for definitions of weak forcing). By examining those three cases separately, we isolate the effect of each forcing mechanism on the cross-shelf flow. For example, to determine the dependence of the cross-shelf velocity profile on the cross-shelf wind stress, we calculated the time-mean cross-shelf velocity profile for cross-shelf wind stress bins covering the full range of observed low-frequency cross-shelf wind stresses (−0.41 to 0.63 Pa). Each velocity profile is a mean over times when τ_s^x is in the wind stress range covered by that bin. It is also a conditional average velocity profile: the time average is taken only over times that satisfy the condition that the along-shelf wind stress and the waves are both small. We then use each average velocity profile to calculate the U_s that corresponds to that cross-shelf wind stress forcing.

3. Models of wind- and wave-driven flow

We compare the observed cross-shelf velocity profiles $u(z, t)$ to the profiles predicted by simple models of wind- and wave-forced flow. The comparison reveals whether the observations are consistent with our understanding of wind and wave forcing, and also whether the existing models are adequate to reproduce ob-

Unauthenticated | Downloaded 10/26/25 08:20 PM UTC

served flows. Finally, we use the process models described below as tools to give a dynamical interpretation of the observations.

a. Model of wind-driven flow

The cross-shelf velocity profile for cross-shelf wind stress forcing in water shallow compared to the boundary layer depth, with a no-slip bottom and a constant eddy viscosity, was found analytically by Ekman (1905) for a two-dimensional velocity field with a horizontal boundary condition of no cross-shelf transport at the coast. That velocity profile has a two-layer structure, with the strongest flow at the surface in the direction of the wind stress and a compensating return flow in the lower layer. To account for the dependence of eddy viscosity on wind stress forcing, we use a slightly more complicated model.

We compare the observed cross-shelf velocity profiles $u(z)$ to the cross-shelf velocity profile $u_\tau(z)$ predicted by a two-dimensional (along-shelf uniform) numerical model with constant density. We use only winter data to compare with the model, because the water column at MVCO is more likely to be unstratified in winter than in summer. The model is described in detail in Lentz (1995). We numerically find the steady solution to the linear momentum equations, with prescribed wind stress and along-shelf pressure-gradient forcing, a coastal boundary condition of zero net cross-shelf flow, and a choice of eddy viscosity profiles. The eddy viscosity in the model depends on the surface and bottom stresses (through the friction velocity), and therefore on the velocity profile. Lentz (1995) considered the cases of forcing by an along-shelf wind stress and an along-shelf pressure gradient. Here, we consider forcing by a cross-shelf or along-shelf wind stress. We use model parameters identical to those given in Lentz (1995). The boundary conditions are applied at a roughness depth or height from the boundary of $z_0 = 1$ cm. The constant eddy viscosity case has $A_\upsilon = 5 \times 10^{-3}$ $m^2\,s^{-1}$. We calculated model results for all the eddy viscosity profiles described in Lentz (1995): constant, bilinear, bilinear cutoff, bilinear decaying exponentially into the interior ("bilinear exponential"), and cubic—as well as for the cubic profile divided by $\sqrt{2}$ (MYApprox). The exact choice of eddy viscosity profile is not important here. The different eddy viscosities are only used to show the range of the predicted cross-shelf velocity response for reasonable choices of the eddy viscosity profile.

We do not expect such a simple numerical model to reproduce exactly the observed cross-shelf flow. The vertical mixing of momentum in reality may depend on the waves, stratification, and surface buoyancy fluxes, none of which is included in the model. The dependence of the vertical mixing of momentum on the wind stress and bottom stress is also likely more complicated than what the model represents with its eddy viscosity profiles. Here, we examine the possibility that the observed cross-shelf flow is driven by a single physical process: forcing by the cross-shelf wind. We therefore use the simplest possible numerical model that can represent that physical process, with the eddy viscosity depending on the wind and bottom stresses in a reasonable way.

To calculate the surface layer transport U_s predicted by the model, we sample the model velocity profile in the same way the ADCP samples the water column. We discard the model velocity profile $u_\tau(z, t)$ above the depth of the top good ADCP bin and below the depth of the bottom good ADCP bin and use a constant velocity profile from those depths to the surface and bottom.

b. Model of wave-driven flow

The companion study Lentz et al. (2008) demonstrates that the observed cross-shelf velocity profiles at MVCO during weak wind stresses in winter match the prediction of Hasselmann (1970) for the Eulerian flow driven by surface gravity waves under the influence of earth's rotation. In that model, the velocity profile u_H is predicted to be equal in magnitude and opposite in sign to the Lagrangian Stokes drift velocity profile u_{st} (Hasselmann 1970), as in Fig. 3:

$$u_H(z, t) = -u_{st}(z, t), \tag{5}$$

where the x component of the Stokes drift due to a monochromatic wave is (Longuet-Higgins 1953)

$$u_{st}(z, t) = \frac{gkH_{sig}^2}{8c} \frac{\cosh[2k(z + h)]}{\sinh(2kh)} \cos\theta_w. \tag{6}$$

The derivation of (5) is reviewed in detail in Xu and Bowen (1994), for example. We use (5) as the model for wave-driven offshore flow (undertow) to compare with the ADCP observations in winter. The depth average of u_{st} calculated from (6) using the observed dominant wave characteristics, which we use here for simplicity, is about 15% larger than the depth average of u_{st} calculated by integrating over the directionally resolved wave spectrum (Lentz et al. 2008).

4. Context

a. Wind stress forcing

Wind direction is reported as degrees counterclockwise from the positive x axis, in the oceanographic con-

Unauthenticated | Downloaded 10/26/25 08:20 PM UTC

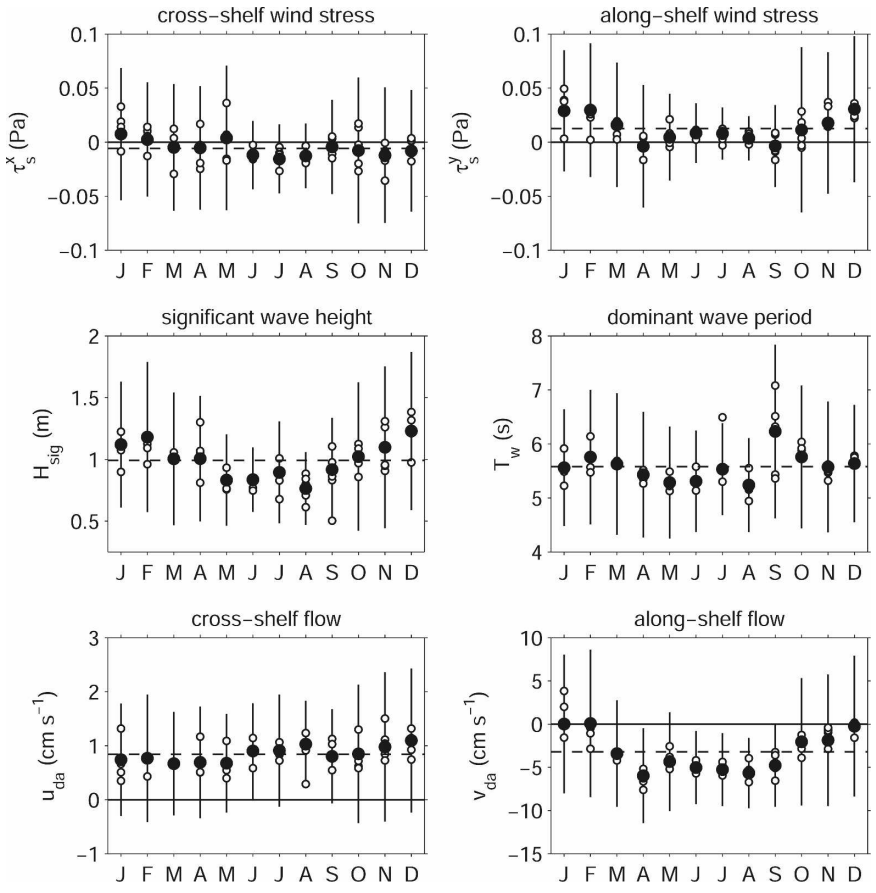

FIG. 4. Monthly (top) mean wind stress, (middle) wave characteristics, and (bottom) depth-average flow at MVCO. Solid dots show the mean over all years. Open circles are individual monthly means for each year separately. Vertical bars show ±1 std dev of the low-pass filtered data for that month, over all years, indicating the strength of synoptic variability. Dashed horizontal line indicates the mean over the entire study period.

vention: an onshore wind is blowing from the sea, toward land. "Upwelling favorable" indicates a wind stress oriented eastward along shelf.

The wind stress forcing near MVCO is dominated by synoptic variability (time scales of a few days, associated with the passage of weather systems) and does not have a large mean value. Monthly mean cross-shelf (along-shelf) wind stresses are no more than 0.02 (0.03) Pa in any season (Fig. 4), and the standard deviations are at least twice as large as the means during all seasons. The mean and variability of the wind stress are larger in winter than in summer. The winds at this site are not strongly polarized, in contrast to the mean upwelling-favorable winds on the west coast of the United States in summer (e.g., Huyer 1983). The standard deviations of the cross-shelf and along-shelf wind stress components at this site have similar magnitudes, about 0.05 Pa.

Here, $|\tau_s^x| < 0.03$ Pa is defined as a small (low-pass filtered) cross-shelf wind, and $|\tau_s^y| < 0.03$ Pa a small along-shelf wind. If we choose a smaller cutoff value, too few data remain for statistically significant calculations in the small wind regime. The total wind stress was small ($|\tau_s| < 0.03$ Pa) 43% of the time.

b. Wave forcing

Both the mean wave forcing and its variability are larger in winter than in summer (Fig. 4). The mean dominant wave period is about 5.5 s, with little seasonal variation. The mean wave forcing is -1.2 m^2, and the standard deviation on subtidal time scales is 1.5 m^2. The wave forcing F_w is almost always negative because $\theta_w \sim 180°$; the wave direction is within 30° of directly onshore 80% of the time (Fig. 5d). The mean (median) dominant wave direction is 179° (202°).

We define small wave forcing as $|F_w| < 0.5$ m^2 ($H_{\text{sig}} \lesssim 0.75$ m). If we choose a smaller cutoff value, too few data remain for statistically significant calculations in

Unauthenticated | Downloaded 10/26/25 08:20 PM UTC

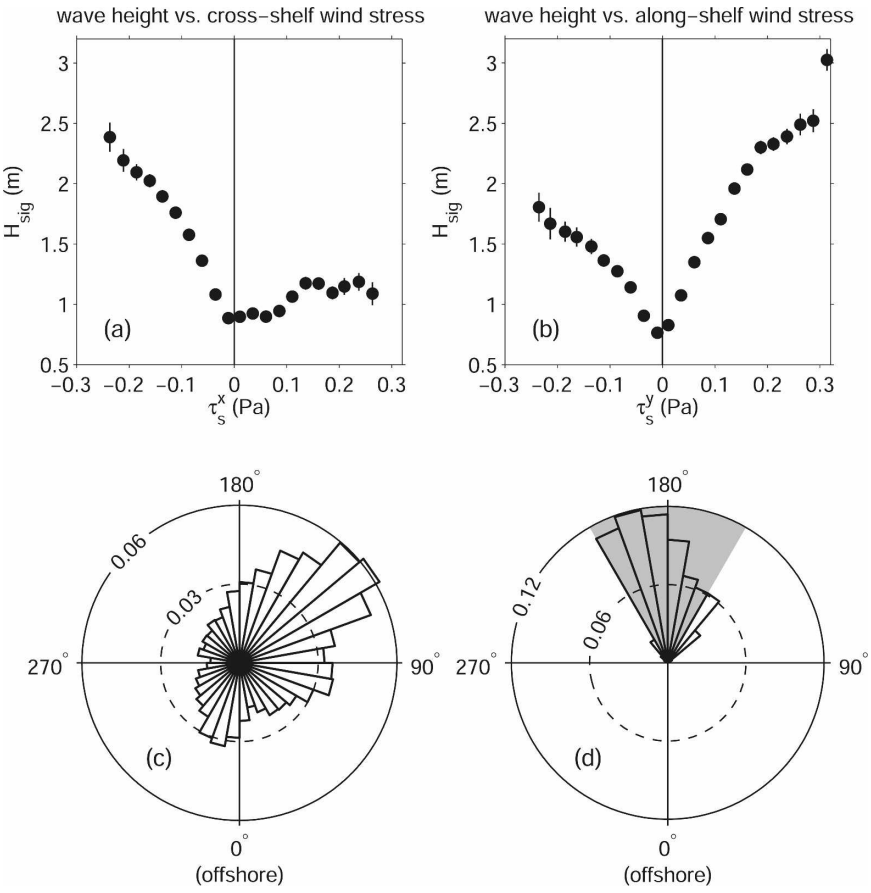

FIG. 5. (top) MVCO significant wave height H_{sig} as a function of (a) cross-shelf wind stress (positive offshore) and (b) along-shelf wind stress (positive = upwelling favorable). (bottom) Normalized histograms of (c) wind stress direction and (d) dominant wave direction (both measured counterclockwise from offshore). Gray shading in (d) indicates directions within ±30° of directly onshore. All panels use low-pass-filtered data.

the small wave regime. The waves are small 40% of the time. Waves and wind stress are both small 24% of the time.

c. *Mean flow*

The time-mean depth-average flow observed by the ADCP is westward and offshore (Fig. 2) and stronger in summer than in winter. The offshore component of the mean flow is almost entirely explained by wave-driven undertow (Lentz et al. 2008) and is therefore consistent with a two-dimensional (along-shelf uniform) circulation. The monthly mean cross-shelf depth-average flow is approximately 1 cm s^{-1} during all seasons (Fig. 4). The monthly mean along-shelf depth-average flow is 1 cm s^{-1} or less westward during November–February, but up to 6 cm s^{-1} westward during April–September. Accordingly, we define summer as 1 April–30 September and winter as 1 October–31 March for this study. The time-mean depth-average flow when waves are small is nearly in the along-shelf westward direction and has a strength of 3 cm s^{-1}, consistent with (but slightly smaller than) the time-mean flows observed at midshelf in this area (Beardsley et al. 1985; Shearman and Lentz 2003; Lentz 2008). Subtidal fluctuations in the depth-average along-shelf flow are strongly correlated with the along-shelf wind stress and seem to be driven by a combination of the along-shelf wind stress and along-shelf pressure gradient, which is also correlated with the along-shelf wind (Fewings 2007). The mean along-shelf flow cannot be driven by the mean along-shelf wind stress, which is eastward, and is likely driven by a mean along-shelf pressure gradient (Lentz 2008).

d. *Wave and wind forcing are correlated*

The three forcing mechanisms considered here (waves, cross-shelf wind, and along-shelf wind) are all correlated (Fig. 5). The correlation coefficient of τ_s^x

Unauthenticated | Downloaded 10/26/25 08:20 PM UTC

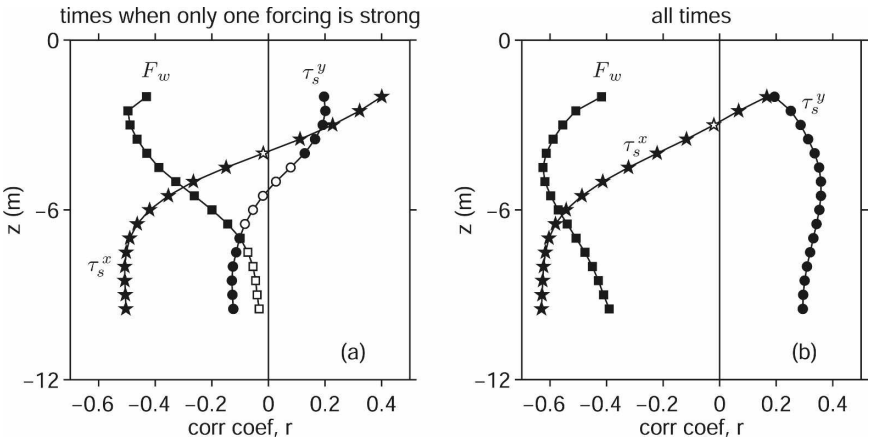

FIG. 6. Correlation coefficient, as a function of ADCP bin depth, of cross-shelf velocity u in each ADCP bin with wave forcing F_w (squares), cross-shelf wind stress τ_s^x (stars), and along-shelf wind stress τ_s^y (circles), at zero lag, assuming one independent point every 24 h, for (a) times when the other two forcing mechanisms are weak and (b) all times. Solid (open) symbols show correlations that are (are not) significant at the 95% confidence level.

with τ_s^y is $r = -0.25$ at zero lag (95% significance level is $|r_s| = 0.04$), but the correlation of onshore wind stress with upwelling-favorable wind stress ($\tau_s^x < 0$ and $\tau_s^y > 0$) is $r = 0.53$ at zero lag ($|r_s| = 0.07$). At this location an upwelling-favorable wind stress is usually associated with an onshore wind stress (Fig. 5c).

The correlation of wind stress magnitude $|\tau_s|$ with wave forcing F_w has a maximum magnitude of $|r| = 0.65$ ($|r_s| = 0.05$) on subtidal time scales, when F_w is lagged 5 h with respect to the wind stress. Offshore wind stresses are generally associated with small waves, but onshore wind stresses are strongly correlated with wave height because the fetch is much larger for onshore than offshore winds (Fig. 5a). Strong along-shelf winds of either direction are associated with large waves (Fig. 5b). These correlations are one reason why it has previously been difficult to separate the influences of waves, cross-shelf wind, and along-shelf wind observationally.

5. Results

a. Correlation of cross-shelf flow with forcing

The cross-shelf flow $u(z, t)$ on the inner shelf at MVCO is significantly linearly correlated at zero lag at the 95% confidence level with the wave forcing F_w and the cross-shelf wind stress τ_s^x, and also with the along-shelf wind stress τ_s^y at a few depths near the surface (Fig. 6a). Although the relation between the wind and wave forcing and the resulting cross-shelf flow is not linear, as discussed below, the linear correlation coefficient gives a crude measure of the strength of the relation. The correlation with along-shelf wind stress, which is the forcing mechanism usually thought to drive cross-shelf exchange via coastal upwelling and downwelling, is the weakest of the three.

The cross-shelf flow in the lower half of the water column is mainly associated with cross-shelf wind stress (onshore flow for offshore winds; Fig. 6a). Cross-shelf flow in the uppermost part of the water column is equally correlated with waves and cross-shelf wind stress.

The results are different when we use all data (Fig. 6b) or use only data from times when one forcing mechanism is strong (Fig. 6a), because the different forcing types are correlated (section 4d) and the responses to wave and cross-shelf wind forcing can cancel each other. Flow is onshore in the top ADCP bins during shoreward winds and offshore during wave forcing (Fig. 6a). Because shoreward winds are correlated with large wave events (Fig. 5), shoreward winds appear unimportant in driving cross-shelf flow in the upper water column unless only times of small waves are considered (cf. solid black stars in Figs. 6a,b). Also, when we consider all times together, the along-shelf wind incorrectly appears to be an important forcing mechanism for cross-shelf flow (Fig. 6b). That is why we initially consider only the events when either wind or wave forcing is strong, but not both, to understand the response of the inner shelf to each forcing mechanism separately.

b. Cross-shelf velocity profiles during weak wind and wave forcing

There is a nonzero cross-shelf velocity present when both waves and winds are weak (Fig. 7a). This "residual" cross-shelf velocity profile is partly due to tides:

Unauthenticated | Downloaded 10/26/25 08:20 PM UTC

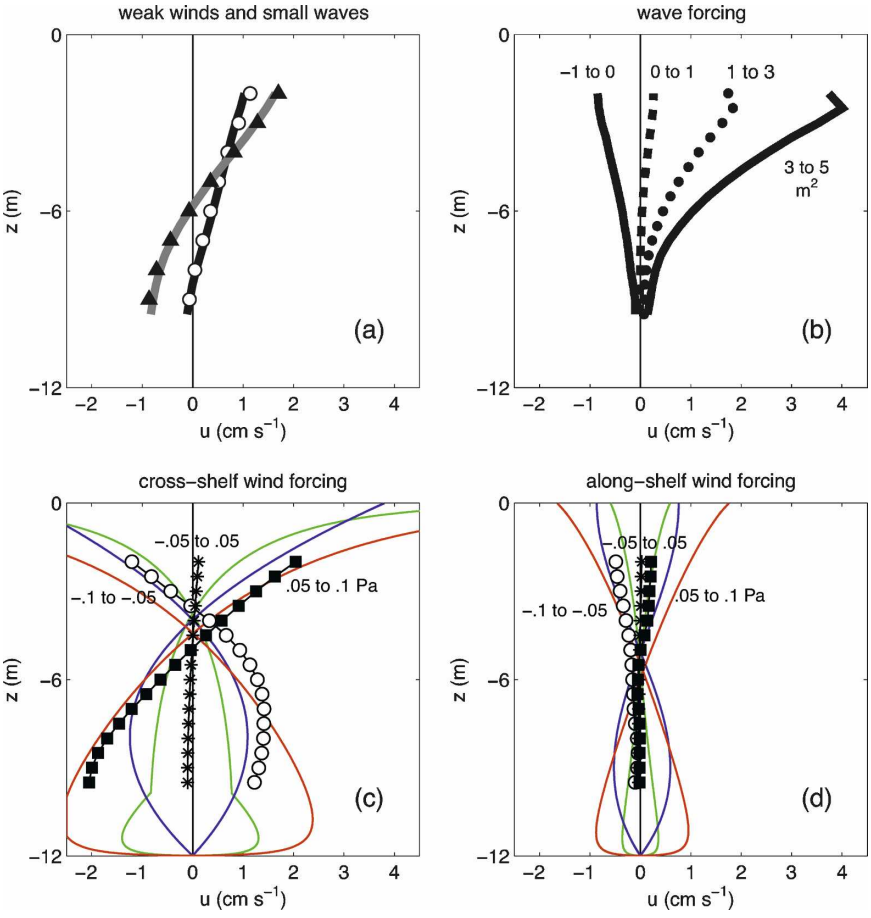

FIG. 7. Vertical profiles of cross-shelf velocity. (a) Mean velocity profile during weak winds and small waves, during spring tides (observed: gray line, and from linear fit to spring-neap index: triangles) and neap tides (observed: black line, and from linear fit to spring-neap index: circles). (b)–(d) Relative to the velocity in (a), the mean velocity for times with (b) $-F_w$ in the ranges shown, during weak winds; (c) τ_s^x in the ranges shown, during small waves and weak along-shelf winds; and (d) τ_s^y in the ranges shown, during small waves and weak cross-shelf winds. In (c) and (d), thin lines are model profiles (section 3a), forced by the mean observed wind stress for each range [in (c), $\tau_s^x = -0.06$ N m^{-2} and $\tau_s^x = 0.07$ N m^{-2}; in (d), $\tau_s^y = -0.07$ N m^{-2} and $\tau_s^y = 0.06$ N m^{-2}], with various eddy viscosity profiles (green = bilinear, blue = constant, red = MYApprox).

it is significantly correlated at the 95% confidence interval with a spring-neap tidal index I_{sn} (defined as the magnitude of the predicted tidal velocity from T_TIDE, low-pass filtered twice with a 33-h cutoff). The velocity during weak waves and winds is stronger during spring tides (0.17 m s$^{-1} \geq I_{sn} \leq$ 0.19 m s^{-1}) than during neap tides (0.12 m s$^{-1} \geq I_{sn} \leq$ 0.14 m s^{-1}) and has a two-layer structure: onshore in the lowest part of the water column, and offshore in the upper part of the water column. It reaches a maximum of nearly 2 cm s^{-1} in the uppermost ADCP bin, and -1 cm s^{-1} in the lowest ADCP bin, during spring tides. Using linear regression of the subtidal cross-shelf flow in each ADCP bin during weak wind and wave forcing against the spring-neap index, we calculated a predicted residual velocity profile that varies in time with the spring-neap index. We subtract that predicted velocity profile from the observed velocity in all of the following analyses, including the velocity profiles shown in Figs. 7b–d. Note that the predicted residual velocity profile includes the intercept from the fit to the spring-neap tidal index. That intercept represents a (relatively small) part of the residual velocity that is not due to tides.

c. *Cross-shelf flow profiles during wind or wave forcing alone*

During wave forcing (when the wind stress is small), the cross-shelf flow is offshore through most of the wa-

Unauthenticated | Downloaded 10/26/25 08:20 PM UTC

ter column below the wave troughs for waves propagating onshore. The flow is surface intensified and stronger during larger waves (Fig. 7b). Onshore-propagating waves generate an offshore flow (undertow) at this location, even though it is 1.5 km offshore, well outside the surfzone ($H_{sig}/h > 0.4$ never occurred and $H_{sig}/h > 0.25$ occurred less than 1% of the time in the unfiltered data). The dependence of the cross-shelf flow on wave forcing at this site is described in Lentz et al. (2008) and will not be detailed here.

During cross-shelf wind stress forcing (when waves and along-shelf wind stress are both small), the cross-shelf flow has a two-layer structure (Fig. 7c). For onshore winds, the flow is onshore in the upper water column and offshore in the lower water column. For offshore winds, the flow is nearly the reverse. The cross-shelf velocity profiles we observe during offshore wind stress forcing are similar to the spatial part of the first empirical orthogonal function (EOF) of the cross-shelf flow observed at 15-m depth on the southern California shelf near the Gaviota mountain pass, where strong offshore winds occur (Cudaback et al. 2005). The temporal part of that EOF is correlated with the cross-shelf wind stress. The zero crossing of the cross-shelf velocity profile at MVCO is at a depth of 4.9–5.5 m (2.7–5.6 m) in winter (summer), approximately one-third to one-half the water depth, for the binned profiles for all cross-shelf wind stress values, except when the wind stress magnitude is less than 0.03 Pa (not shown). This is consistent with the modeled u_τ (section 3a), which has its zero crossing at a depth of 4.6–4.7 m for wind stress values $0.05 < |\tau_s^x| < 0.25$ Pa. The model predictions of the cross-shelf velocity profiles u_τ compare reasonably well with the average observed profiles for both onshore and offshore wind stresses, considering that the model parameters were not adjusted to maximize the fit to the data (Fig. 7c). The model velocity profiles are shown for the bilinear, constant, and MYApprox eddy viscosity profiles, for $\tau_s^x = -0.06$ and 0.07 Pa, which are the mean observed τ_s^x values for the wind stress ranges -0.1 Pa $< \tau_s^x < -0.05$ Pa and 0.05 Pa $< \tau_s^x < 0.1$ Pa, respectively. The bilinear (green) and MYApprox (red) profiles span the range of model velocity profiles yielded by all the different eddy viscosity forms. The bilinear cutoff and cubic (not shown; similar to MYApprox but slightly smaller) and MYApprox (red) eddy viscosity profiles give the best agreement with the data in the offshore wind case. The constant eddy viscosity (blue) gives the best agreement in the onshore wind case, but too small a response in the lower water column during offshore wind. The bilinear (green) and bilinear exponential (not shown) profiles lead to a kink in the cross-shelf velocity during cross-shelf wind forcing, for the parameters from Lentz (1995). Note that we are comparing model velocity profiles to only part of the observed velocity profile (because the predicted residual velocity profile due to tides and during weak waves and winds was subtracted), even though the eddy viscosity in the model is a nonlinear function of the velocity profile. Nevertheless, model calculations of the velocity profile with wind and wave forcing together are similar to the sum of model calculations with wind or wave forcing only (section 5d), except very near the surface where the shear is large, indicating that the effect of neglecting turbulent mixing due to the shear in the residual velocity (which is smaller than the shear in the wave-driven profiles) is likely small.

During along-shelf wind stress forcing (when waves and cross-shelf wind stress are both small), the cross-shelf flow displays essentially no response (Fig. 7d). This is in contrast to typical midshelf sites, where the along-shelf wind stress is the dominant component of wind forcing, and drives a coastal upwelling or downwelling circulation. At MVCO, along-shelf winds do not generate as large a cross-shelf circulation as do cross-shelf winds (or waves or tides).

The observed profiles during along-shelf wind stress forcing are roughly consistent with the predicted u_τ when the model is driven with an along-shelf wind stress; the model profiles are shown in Fig. 7d for $\tau_s^y = -0.07$ Pa and $\tau_s^y = 0.06$ Pa, which are the mean observed τ_s^y values for the wind stress ranges -0.1 Pa $< \tau_s^y < -0.05$ Pa and 0.05 Pa $< \tau_s^y < 0.1$ Pa, respectively. The model predicts a small response of the cross-shelf circulation to along-shelf wind forcing at this water depth, in agreement with the observed (lack of) response.

d. Cross-shelf profiles during combined forcing

We also examined the cross-shelf velocity profiles during times when both cross-shelf wind and wave forcing were strong. Onshore winds rarely occur without substantial wave forcing, and offshore winds are sometimes accompanied by remotely generated waves propagating onshore, so it is important to understand the response to combined forcing.

We compare the observed profiles during combined forcing to a simple model, in which we assume that the velocity profile during combined forcing, $u_{\tau+H}$, is the sum of the model profiles during separate forcing (sections 3a, b):

$$u_{\tau+H} = u_\tau + u_H, \tag{7}$$

where u_τ is the modeled velocity due to wind forcing only and u_H is the modeled velocity due to wave forcing

Unauthenticated | Downloaded 10/26/25 08:20 PM UTC

only [see (5)]. Another approach is to incorporate the wave forcing into the numerical model of Lentz (1995), so that the wave-driven flow influences the surface and bottom stresses and therefore the eddy viscosity profile that determines the wind-driven response u_τ. We find that approach gives results very similar to (7) for all but the largest wave forcing, in which case the profile predicted by the combined model is less vertically sheared near the surface than the linear superposition in (7). For simplicity, we use (7) to compare with the observations. In this section, we use the cubic eddy viscosity profile, which fits the profiles during cross-shelf wind forcing reasonably well (section 5c).

The comparison of $u_{\tau+H}$ with observed mean profiles is shown in Fig. 8 for several representative forcing regimes, using winter data only because the wind-driven model is unstratified. We subtracted from the observations both the residual velocity profile (section 5b; Fig. 7a) and the part of the depth-average flow that differed from the depth average of u_H in each case (similar to section 2f).

Although the mean observed wave height is constant within each row in Fig. 8, the wave-driven circulation (dotted lines) decreases from left to right in each row, as the wind goes from onshore to offshore and the fetch decreases (e.g., compare the top left and top right in Fig. 8). This is because as the wind goes from onshore to offshore, the dominant wave period T_w increases, so the phase speed c increases, and both Q_w and u_H decrease (sections 2d, 3b). The increase in wave period for offshore winds is at first counterintuitive because the fetch is smaller for offshore winds. The explanation involves the presence of both wind waves (small T_w) and swell (large T_w). The wave height H_{sig} is calculated from the total energy in the water velocity spectrum. The amount of energy in the wind–wave part of that spectrum is smaller for smaller fetch (offshore winds). Therefore, for a given H_{sig} (along a row in Fig. 8), more of the wave energy is due to remotely generated swell during offshore winds, so the dominant T_w is larger and the predicted wave-driven circulation is smaller for offshore winds.

The circulation driven by the cross-shelf wind stress during small waves (bottom row of Fig. 8) is roughly symmetric in the wind direction, as discussed in section 5c. As the wave forcing increases (going from the bottom to the top row in Fig. 8), however, the roughly symmetric wind-driven circulation evident in the bottom row is gradually overwhelmed by the wave-driven undertow, which is always directed offshore (as in the middle column). Therefore, during strong wave forcing (top row of Fig. 8), the cross-shelf circulation is no longer symmetric in the wind direction: the cross-shelf velocity profile is nearly vertically uniform for large waves and onshore winds because the vertical shears are similar in magnitude but of opposite sign, while for large waves and offshore winds the velocity profile is strongly sheared because the wave- and wind-driven shears are large and of the same sign. The observed velocity profiles during combined cross-shelf wind and strong wave forcing range from vertically uniform (top left) to a profile with a depth-dependent part that looks like an upwelling circulation (top right).

The response to combined wind and wave forcing is roughly a linear combination of the separate responses u_τ to wind forcing and u_H to wave forcing (Fig. 8; Lentz et al. 2008). The discrepancy between the modeled and observed profiles is larger in summer than in winter (not shown); in summer, the observed profiles are more vertically sheared than in Fig. 8, but the model profiles are the same because the models do not depend on stratification. The linear correlation between the model $u_{\tau+H}(z, t)$ and the observations $u(z, t)$ at any one depth is $r_W = 0.76$ in winter and $r_S = 0.57$ in summer (average correlation coefficient for all depths, all correlations at zero lag), and the 95% confidence level is $r_s = 0.07$–0.08 in both cases. At middepth in winter, the correlation is $r = 0.83$. Therefore, the model $u_{\tau+H}(z, t)$ explains 58% of the subtidal variance in the cross-shelf velocity on average in winter ($r_W^2 = 0.58$) and as much as 69% of the variance at middepth.

e. Cross-shelf transport in the upper layer

Because the flow has a two-layer structure during cross-shelf wind forcing (Figs. 7c, 8, bottom row), the dependence of the cross-shelf flow profile on wind forcing can be quantitatively characterized by the volume transport in the upper layer, U_s. The residual velocity profile described in section 5b (Fig. 7a) is subtracted from the observed profile before calculating U_s.

A substantial cross-shelf transport is associated with cross-shelf winds (Fig. 9a). We observe an approximately linear relation between the strength of the cross-shelf transport and the cross-shelf wind stress over the range of wind stress values observed when waves are small, during both summer and winter. There were few times when the cross-shelf wind stress was strongly onshore but the waves were small (Fig. 5a), so the observations do not extend to very large negative values of τ_s^x. The upper-layer cross-shelf transport response is approximately twice as large in summer as in winter (Fig. 9a) for a given strength of offshore wind stress.

The cross-shelf transport observed during onshore or offshore wind forcing in winter is small compared to the transport expected at midshelf (dashed and dotted lines in Fig. 9a), except during very weak cross-shelf wind

Unauthenticated | Downloaded 10/26/25 08:20 PM UTC

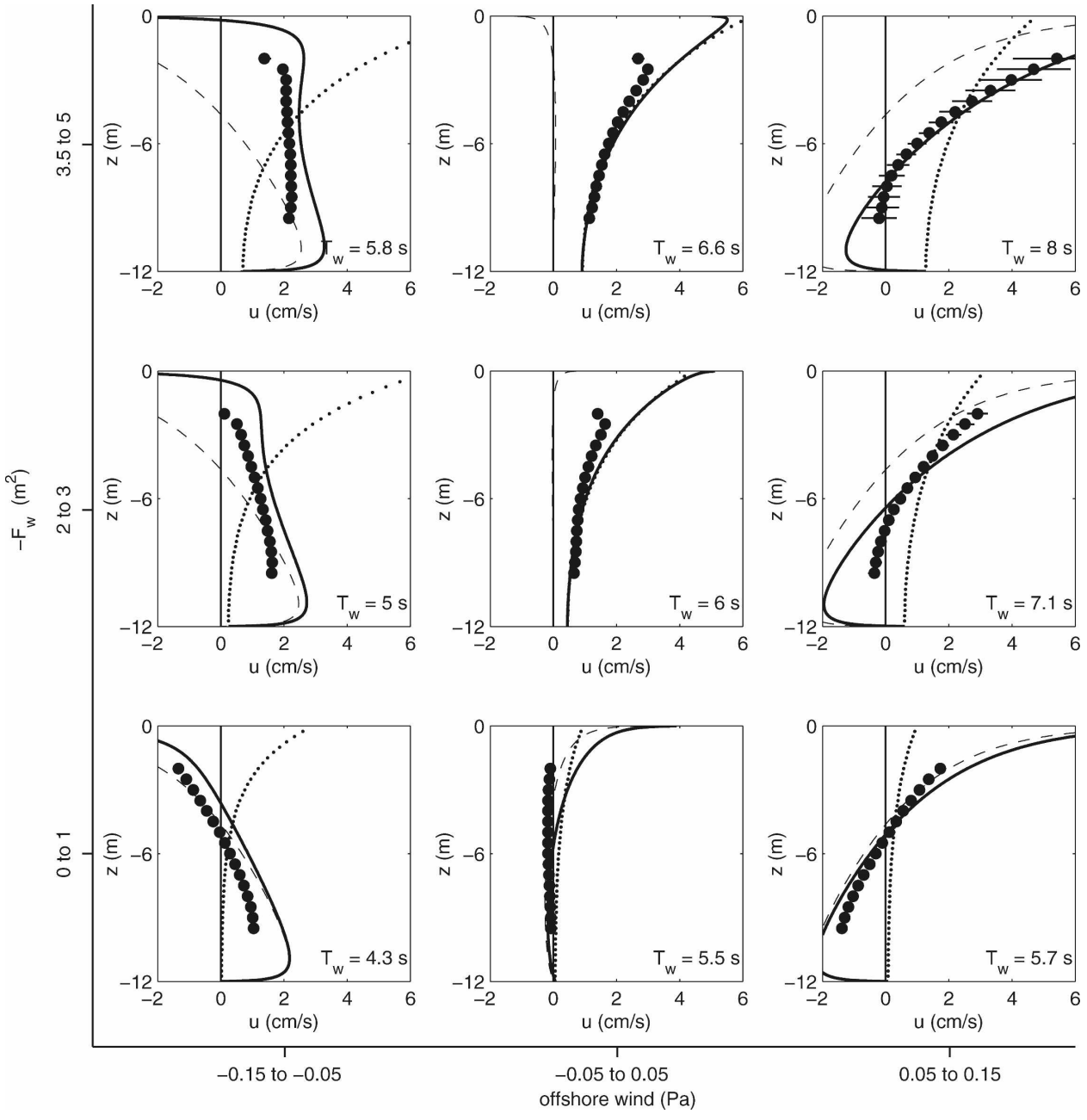

FIG. 8. Vertical profiles of cross-shelf velocity during various forcing conditions in winter. Wave forcing increases from bottom to top. Wind stress is (left) onshore, (middle) small, or (right) offshore. Black circles: mean observed profiles; the part of u_{da} that differs from the predicted depth-average u_H was subtracted. Dotted lines: predicted wave-driven flow, u_H (section 3b). Dashed: predicted wind-driven flow u_τ, using the cubic eddy viscosity profile (section 3a). Solid lines: $u_{\tau+H}$. If the models are correct, the observations should fall on the solid lines. The mean observed wave period T_w is given in each case.

stress ($0 < \tau_s^x < 0.004$ Pa). [The maximum predicted $U_s/\tau_s^x \rho_0 f$ for cross-shelf wind is larger than 0.2, and up to at least 0.45, for eddy viscosities that are not constant vertically, based on the numerical model in Lentz (1995).] The small cross-shelf transport at MVCO is consistent with the idea that this site at 12-m water depth is within the inner shelf for all but the smallest wind stresses in winter.

We use the model prediction for wave-driven flow to extend the plot of U_s versus τ_s^x in winter beyond the range of Fig. 9 to larger values of wind stress, when waves are generally present. To do this, we consider all

Unauthenticated | Downloaded 10/26/25 08:20 PM UTC

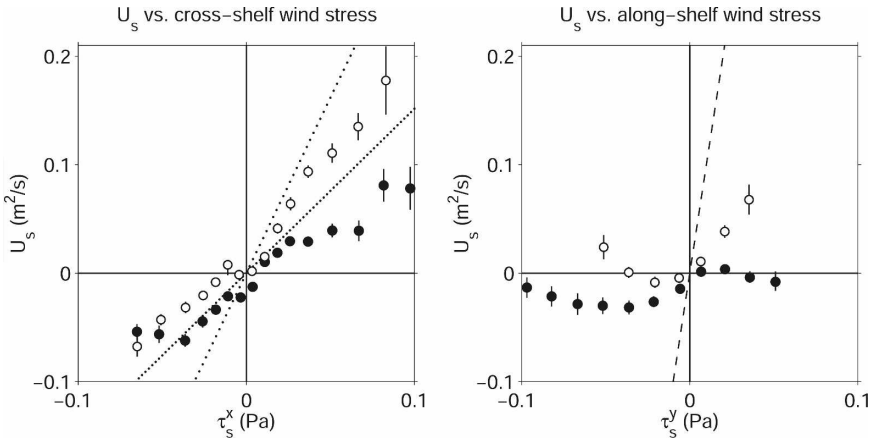

FIG. 9. Cross-shelf transport in the upper water column during summer (open symbols) and winter (closed symbols), as a function of (left) cross-shelf and (right) along-shelf wind stress, during times when waves were small and the other wind component was weak in each case. Error bars are ±1 standard error of the mean [for details, see Fewings (2007)]. Dashed and dotted lines indicate deep-water Ekman transport values: (right) $U_s = \tau_s^y/\rho_0 f$ for along-shelf wind (Ekman 1905) and (left) $U_s = 0.2\tau_s^x/\rho_0 f$ or $0.32\tau_s^x/\rho_0 f$ for cross-shelf wind, from Weatherly and Martin (1978), with a modified coefficient of 0.32 for this definition of U_s from Tilburg (2003), or 0.2 based on Lentz (1995).

wave conditions, and subtract from the observed velocity profile the predicted wave-driven velocity profile u_H (section 3b). We then calculate an extended surface layer transport U_s' from the resulting $u(z, t) - u_H(z, t)$ in the same manner as in section 2f. The extended transport U_s' compares well with the observed U_s during small waves in winter, where the two sets of data overlap (cf. open and closed symbols, Fig. 10). The transport U_s' is approximately symmetric with respect to the cross-shelf wind direction (Fig. 10, left). With the extended range of wind stress, we can see that the response is not actually linear for onshore (negative) wind stresses. For small cross-shelf wind stresses, $|\tau_s^x| < 0.04$ Pa, the response is approximately linear in τ_s^x. For $|\tau_s^x| > 0.04$ Pa, however, $|U_s'|$ increases more slowly with increasing $|\tau_s^x|$.

The reduced slope of U_s' versus τ_s^x for large onshore wind stress forcing (Fig. 10) can be thought of as being caused by increasing overlap of the top and bottom boundary layers for increasing wind stress, and a resulting shutdown of the wind-driven response. This is consistent with the idea that when the wind stress (cross shelf or total) becomes large, the top and bottom boundary layers overlap to the extent that vertical transfer of momentum through the water column is extremely rapid and the eddy viscosity is large throughout the water column. Then the shear in the cross-shelf velocity is reduced, and U_s (or U_s') does not increase as rapidly with wind stress as it does for small wind forcing. The numerical model crudely represents this process, and the model predictions agree with the observed U_s. This model-data agreement suggests that the cross-shelf velocity response we observe at MVCO during cross-shelf wind stress forcing is indeed a response to the cross-shelf wind stress, not to some other forcing that is simply correlated with cross-shelf wind stress.

To compare the surface layer transport from the unstratified model with the observations, we used winter data only. In winter, however, the surface heat flux is often cooling the ocean and the water column may be actively convecting rather than simply unstratified. In that case, with enhanced vertical mixing of momentum, we would expect a decreased cross-shelf transport response. Indeed, the surface transport U_s during offshore winds in winter is smaller when we consider only times when the ocean is strongly cooling (surface heat flux more negative than -50 W m^{-2}, not shown).

We observe almost no dependence of the cross-shelf transport U_s on the along-shelf wind stress during winter (Figs. 9b, 10b). There seems to be a weak nonzero cross-shelf transport associated with upwelling-favorable wind forcing in summer, although there are very few events with upwelling-favorable wind stress but weak cross-shelf wind and small waves (Fig. 9b). There is also some indication of onshore transport in the surface layer (a downwelling circulation) during downwelling-favorable wind stress in summer at times when the surface heat flux is positive (>50 W m^{-2}, not shown). It is unclear whether the data extended to all wave conditions (Fig. 10b, open circles) actually represent the response to along-shelf wind forcing (it seems unlikely that upwelling-favorable wind causes a down-

Unauthenticated | Downloaded 10/26/25 08:20 PM UTC

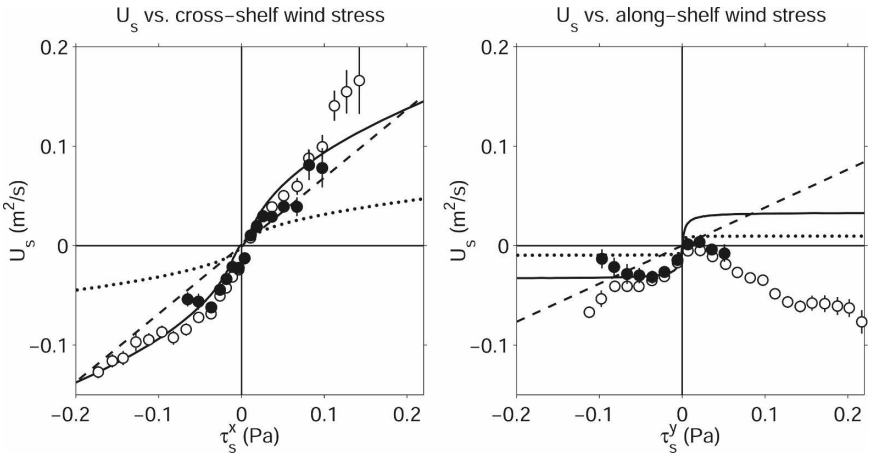

FIG. 10. Cross-shelf transport in the upper water column, U_s (positive offshore), as a function of (left) cross-shelf or (right) along-shelf wind stress, during winter. Solid symbols: U_s during small waves and weak $|\tau_s^y|$ (left) or $|\tau_s^x|$ (right). Open symbols: U_s', which is U_s during any wave conditions and weak $|\tau_s^y|$ (left) or $|\tau_s^x|$ (right), but with the predicted wave-driven velocity profile $u_H(z, t) = -u_{st}(z, t)$ (Hasselmann 1970) subtracted from $u(z, t)$ before calculating U_s. Error bars are ± 1 standard error of the mean. Lines indicate the U_s predicted by a simple numerical model with constant density and various eddy viscosity profiles (dotted = bilinear, dashed = constant, solid = MYApprox), forced by (left) cross-shelf or (right) along-shelf wind stress (Lentz 1995).

welling circulation in winter) or are artifacts of the small but finite cross-shelf wind forcing, or inaccuracy of the wave model (the surface heat flux was cooling the ocean during those events, and the strong vertical mixing probably associated with that surface cooling is neglected by the wave model, so the subtracted wave-driven flow prediction may be an overestimate). Nevertheless, both the observed and the predicted responses to along-shelf wind stress are small for this water depth. The observed and modeled U_s for along-shelf wind stress (Fig. 10b, solid symbols and solid or dotted line) do agree reasonably well, considering that the signal of U_s versus τ_s^y is so weak.

f. Along-shelf flow profiles

There is also a residual along-shelf flow during weak wind and wave forcing that is correlated with the spring-neap index (Fig. 11a). We subtracted a predicted along-shelf flow profile based on the spring-neap index before calculating the along-shelf flow profiles in Figs. 11b–d. Note that the residual along-shelf flow in Fig. 11a could be partly driven by an along-shelf pressure gradient rather than by tides alone. The remaining along-shelf velocity profiles are nearly vertically uniform during wave forcing (Fig. 11b), with the flow becoming more westward with increasing wave forcing. The along-shelf flow during cross-shelf wind forcing (Fig. 11c) is weak compared to during along-shelf wind forcing (Fig. 11d), consistent with the idea that the cross-shelf wind is ineffective at driving along-shelf flows over the continental shelf (e.g., Csanady 1978; Allen 1980; Brink 1998). The along-shelf wind appears to be the main driving mechanism for the fluctuating subtidal along-shelf flow. This is consistent with a depth-average subtidal along-shelf momentum budget near MVCO (Fewings 2007), which indicates that the along-shelf flow is mainly driven by the along-shelf wind stress and an along-shelf barotropic pressure gradient due partly to the along-shelf wind stress, in agreement with Lentz (2008).

6. Discussion

a. Importance of along-shelf wind

The importance of cross-shelf wind forcing at MVCO leads us to reexamine the results of previous inner-shelf studies. Observational studies on the North Carolina and Oregon shelves demonstrated a divergence across the inner shelf in the cross-shelf transport associated with along-shelf wind stress (Lentz 2001; Kirincich et al. 2005). In both cases, the authors used the entire available time series to calculate a correlation between the surface layer transport U_s and the along-shelf wind stress at each water depth, because the time series were too short to separate into events where only one wind component was strong. The along-shelf and cross-shelf

Unauthenticated | Downloaded 10/26/25 08:20 PM UTC

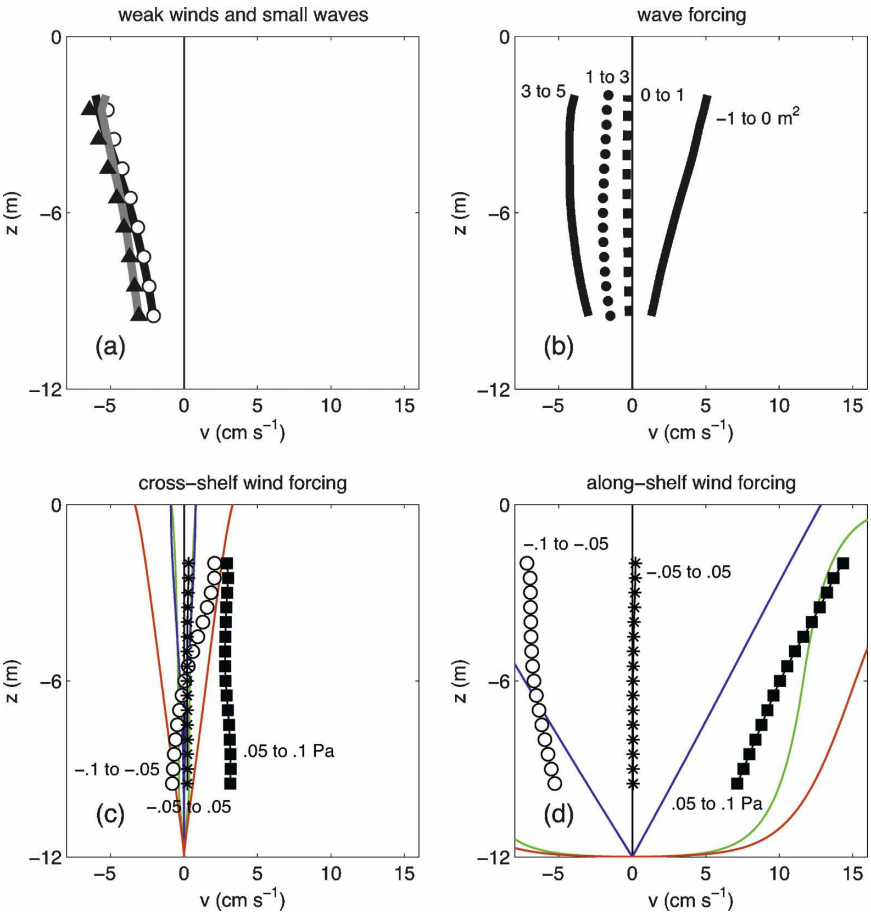

FIG. 11. Same as in Fig. 7, but showing profiles of along-shelf velocity.

wind stress components can be correlated (section 4d). As a result, the importance of the along-shelf wind stress in driving a cross-shelf circulation may be overestimated in those studies (as in Fig. 6b). We suggest that the cross-shelf Ekman transport U_s associated with the along-shelf wind on the North Carolina inner shelf may decrease even faster with decreasing water depth than demonstrated in Lentz (2001), because the subtidal cross-shelf and along-shelf wind stress components at that site are significantly positively correlated (Austin and Lentz 1999). Therefore, a substantial fraction of the transport U_s attributed to along-shelf wind stress forcing at the North Carolina site may actually be due to cross-shelf wind stress. The cross-shelf wind stress probably does not contribute as much to U_s on the Oregon coast, where the wind stress is more polarized in the along-shelf direction.

b. Comparison to 2D model

A recent numerical model study (Tilburg 2003) shows that when the water depth is small enough for substantial overlap of the surface and bottom boundary layers, the cross-shelf wind stress drives a stronger cross-shelf surface layer transport than does the along-shelf wind stress. Tilburg ran the model in a two-dimensional (along-shelf uniform) configuration, with initially linear stratification and a Mellor–Yamada level 2.5 turbulence closure scheme. For a constant wind stress magnitude, as a function of wind angle, the cross-shelf surface layer transport in that model was greatest for cross-shelf wind and zero for along-shelf wind in the very shallow inner shelf (5-m water depth).

We observe a similar dependence of surface layer transport on wind stress angle, for a given range of wind stress magnitude, during small waves (Fig. 12). We consider winter data only, to minimize the effects of stratification. The largest cross-shelf surface layer transport occurs for wind stress in the offshore or nearly onshore direction, and that surface layer transport is in the same direction as the wind stress. The weakest cross-shelf surface layer transport occurs when the wind stress is in the upwelling- or downwelling-favorable (along-shelf)

Unauthenticated | Downloaded 10/26/25 08:20 PM UTC

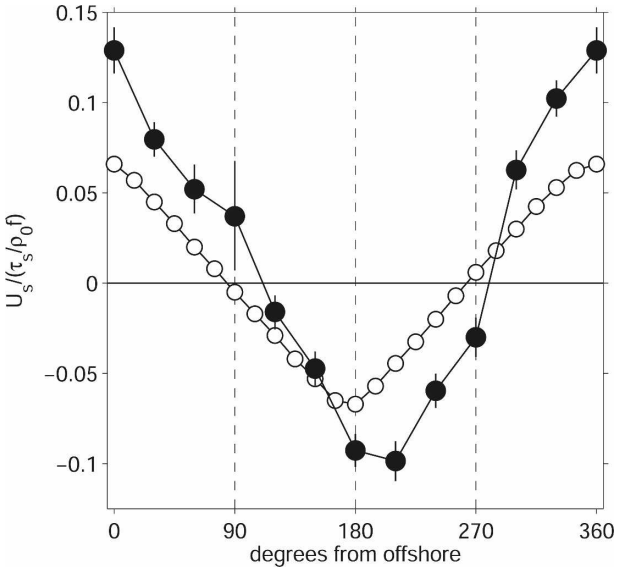

FIG. 12. Normalized cross-shelf transport in the surface layer, $U_s/(|\tau_s|/\rho_0 f)$ (positive offshore), as a function of wind direction. Open circles: numerical model results for $|\boldsymbol{\tau}_s| = 0.1$ Pa and $h = 5$ m [taken from Tilburg's (2003) Fig. 16]. Solid symbols: MVCO observations for $h = 12$ m and $0.04 < |\boldsymbol{\tau}_s| < 0.15$ Pa. The cross-shelf velocity profiles were bin averaged by wind direction, then U_s was calculated, then normalized by the bin-averaged $|\boldsymbol{\tau}_s|/\rho_0 f$. These data are restricted to times when waves are small, so there are fewer events for the onshore wind stress angles (near 180°) than for the offshore. In both the model and the observations, the largest surface layer transport is for cross-shelf, not along-shelf, winds.

direction. The U_s we observe is slightly larger than that predicted by Tilburg (2003) for onshore winds. His model run was for a water depth of 5 m, however, as opposed to the MVCO water depth of 12 m, and U_s is expected to increase with increasing water depth in the inner shelf, even in the region where the maximum upper-layer transport is downwind (Fig. 15).

Tilburg (2003) gives an estimate for the depth of the first zero crossing of the cross-shelf flow at midshelf, δ, as a function of wind stress and stratification [his Eq. (22)]. Tilburg uses the formula of Weatherly and Martin (1978), but with an adjusted coefficient to match his definition of U_s based on the first zero crossing of the cross-shelf velocity (as in this study) rather than on the full boundary layer depth:

$$\delta = 2.3\sqrt{\frac{|\tau_s|}{\rho_0}}\frac{1}{f(1 + N^2/f^2)^{1/4}}, \qquad (8)$$

where $N = [(-g/\rho_0)(\partial\rho/\partial z)]^{1/2}$ is the buoyancy frequency. If δ is larger than the water depth, Tilburg predicts a circulation governed by inner-shelf dynamics and not midshelf dynamics. For an unstratified water column ($N = 0$), (8) predicts $\delta > h$ at MVCO for $|\boldsymbol{\tau}_s| \geq 3 \times 10^{-4}$ Pa. For a typical summertime value *of* $N = 0.02$ s^{-1} in the Middle Atlantic Bight (Linder and Gawarkiewicz 1998), (8) predicts $\delta > h$ at MVCO for $|\tau_S| \geq 0.05$ Pa. This is consistent with the MVCO site being in the inner shelf nearly all the time, except during extremely weak winds when the water column is strongly stratified. Indeed, it is only during summer that U_s approaches the predicted midshelf value for a given cross-shelf wind stress (cf. dotted line and summer observations in Fig. 9).

c. Comparison to unstratified model

There appears to be a slight asymmetry between the responses to onshore and offshore winds (Fig. 10, left). With the available observations (which do not include density profiles for the entire time series) we cannot determine whether the slight asymmetry in Fig. 10 is caused only by differences in surface heat flux or stratification between events, and therefore not directly caused by the cross-shelf wind stress, or whether there is an inherent asymmetry in the response of the system to cross-shelf wind stresses of opposite directions.

Another possible explanation for the asymmetry in Fig. 10 is uncertainty in the wind stress estimates. The bulk formula used here (section 2a) uses the same drag coefficient for all wind directions, even though the MVCO study location has land nearby to the north and water to the south, and the drag coefficient should be larger over land than water. The atmospheric boundary layer may still be adjusting over the 12-m isobath at MVCO (1.5 km offshore) when the wind is blowing from land. Further, the adjusted wind stress time series from the MVCO shore masts (Fewings 2007, her appendix A) may still not accurately represent the wind stress at the 12-m isobath. Also, when the wind is in the same direction as the wave propagation, the effective wind stress should be smaller than when the wind is against the waves, but we do not take that into account here.

d. Seasonal change in the response to wind

Stratification is expected to affect the cross-shelf circulation by suppressing vertical mixing, and therefore thinning the surface and bottom boundary layers and reducing their overlap. This would cause the boundary between the inner shelf and the midshelf to move closer to shore. As long as that boundary remains offshore of the 12-m isobath, we would expect a stronger cross-shelf circulation at MVCO (for either wind direction) during stronger stratification, as a result of decreased boundary layer overlap, based on section 6c.

Although the long MVCO velocity time series does

Unauthenticated | Downloaded 10/26/25 08:20 PM UTC

not have associated stratification data, at MVCO the water is typically more stratified in summer than in winter. The cross-shelf wind does drive a larger cross-shelf transport U_s in summer than in winter (Fig. 9, left). In summer, U_s does appear to approach the mid-shelf (deep water) limit for offshore winds at least as large as 0.08 Pa (dotted lines in top right in Fig. 9a). This is consistent with the expected response to increased stratification, which may play an important role by reducing the overlap of the surface and bottom boundary layers.

The cross-shelf transport associated with along-shelf wind may be nonzero during upwelling-favorable wind stress forcing in summer, even though it is zero in winter (Fig. 9, right). This is consistent with the expected response to increased stratification, if the MVCO site is within the inner shelf and therefore the transport associated with along-shelf wind is insignificant when stratification is weak (in winter or during downwelling-favorable winds, which could destroy the stratification in summer). Upwelling can bring colder, denser water onshore near the bottom of the water column, thereby maintaining the summer stratification and the reduced boundary layer overlap. The MVCO site seems to be closer to midshelf in summer during upwelling-favorable or offshore winds than in winter or during downwelling-favorable or onshore winds.

e. Implications for Lagrangian particle transport

The observed cross-shelf transport may seem weak ($U_s < 0.2$ m^2 s^{-1}), but it is enough to flush the entire volume of the inner shelf onshore of the 12-m isobath in about 1 day. Therefore, the cross-shelf wind-driven shear flows we observe are strong enough to change the density stratification of the inner shelf on biologically and physically relevant time scales and to have significant effects on the inner-shelf transport of heat, salt, larvae, nutrients, phytoplankton, pollutants, and carbon. Note, however, that the Eulerian cross-shelf velocity profiles discussed up to this point are not the same as the Lagrangian water parcel velocities. It is the Lagrangian velocity—the velocity of a particle in the water column—that matters for tracer transport. The Lagrangian particle velocities may be very different from the Eulerian velocities as a result of surface gravity waves.

In particular, waves induce a net particle velocity, the Stokes drift $u_{st}(z, t)$ [see (6)], in the direction of wave propagation (Stokes 1847), as in Fig. 3 (right). We form an estimate of the total Lagrangian particle velocity $u_L(z, t)$ by adding the Stokes drift to the observed Eulerian velocity response to wind and waves:

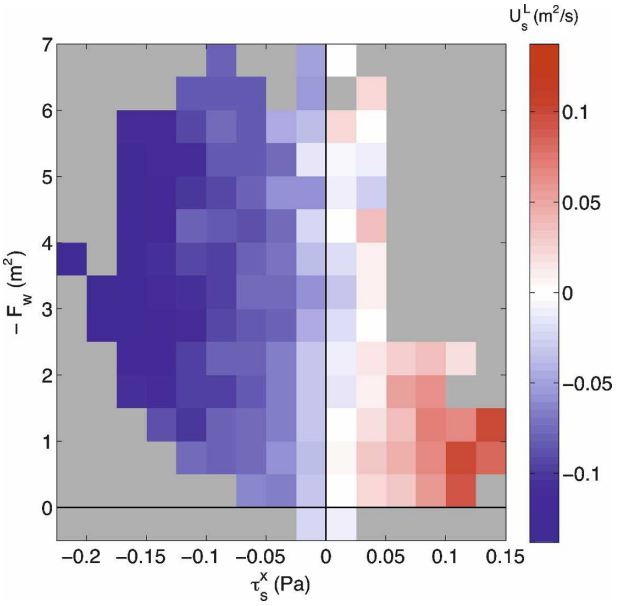

FIG. 13. Estimated Lagrangian cross-shelf surface layer transport U_s^L in winter, as a function of cross-shelf wind stress τ_s^x and wave forcing F_w. U_s^L is calculated in the same way as U_s, but from the estimated Lagrangian velocity profile $u_L(z, t) = u(z, t) + u_{st}(z, t)$. Red (blue) indicates offshore (onshore) surface layer transport, which has the sense of upwelling (downwelling). Gray areas indicate forcing regimes that had fewer than 10 independent events. Most of the time, the system is in the lower central part of the diagram. As a result, although the downwelling region in the figure is larger than the upwelling region, the time-mean U_s^L is very small (-0.03 m^2 s^{-1}). The time-mean Lagrangian circulation by this crude estimate is essentially zero in winter.

$$u_L(z, t) \approx u(z, t) + u_{st}(z, t). \quad (9)$$

We estimated the Lagrangian cross-shelf transport in the surface layer, U_s^L, from u_L in the manner of section 2f, first subtracting the residual velocity profile (section 5b) from $u(z, t)$.

Waves should cause a significant difference between the Eulerian circulation and the Lagrangian particle velocities at this site. The estimated Lagrangian cross-shelf transport in winter is approximately the same as the Eulerian response to wind, even during strong wave forcing (Fig. 13). The result is as if the incoming waves affected the Eulerian circulation but not the Lagrangian velocities. This is because the observed wave-driven Eulerian offshore flow is approximately equal to the Hasselmann (1970) prediction u_H in winter (Lentz et al. 2008) and $u_H(z, t) = -u_{st}(z, t)$ (Fig. 3, right). Therefore, the wave-induced Stokes drift tends to cancel the wave-driven undertow throughout the water column in winter. As a result, the Lagrangian particle velocities are likely similar to the Eulerian cross-shelf velocities driven by cross-shelf wind stress alone.

Unauthenticated | Downloaded 10/26/25 08:20 PM UTC

This is consistent with the nonacceleration theorem, in which a statistically steady eddy or wave field does not accelerate a mean flow in a generalized Lagrangian mean sense (Andrews and McIntyre 1976).

7. Summary and conclusions

The forcing mechanisms for cross-shelf exchange on the inner shelf are fundamentally different from those at midshelf. A 6-yr-long time series of wind, wave, and ADCP velocity data from the cabled MVCO observatory contains enough different wave and meteorological forcing events that we are able to observe, for the first time, the dependence of the cross-shelf flow profile on cross-shelf wind or along-shelf wind alone. We remove tidal and tidal residual circulations. The cross-shelf wind, not the along-shelf wind, is the main forcing mechanism for subtidal cross-shelf circulation at this site when waves are small, especially in winter (Fig. 14, bottom). This is in contrast to coastal upwelling and downwelling driven by along-shelf winds in deeper water at midshelf (Fig. 14, top).

There is a two-layer flow structure associated with cross-shelf wind forcing, with offshore flow in the surface layer for offshore winds and a compensating return flow in the lower layer. The zero crossing of the velocity is at approximately one-third the water depth, in agreement with simple models. The circulation is nearly symmetric in the wind stress direction when the wave forcing is small. In winter, the volume transport in the surface or bottom layer agrees with unstratified models of cross-shelf wind stress forcing. In summer, when stratification is stronger than in winter, a given cross-shelf wind stress is associated with a stronger (more vertically sheared) cross-shelf circulation than in winter.

The cross-shelf velocity profile during combined wave and wind forcing is approximately a linear superposition of the separate responses to cross-shelf wind and to waves. The combined wave and wind forcing yields an asymmetry in the response with respect to cross-shelf wind direction. During large waves, the circulation is vertically uniform for onshore winds but strongly sheared for offshore winds. The relative importance of wind and wave forcing depends on water depth. Progressing from the outer edge of the surfzone through the inner shelf toward midshelf, as the water depth increases, the circulation—aside from tidally driven motions—is dominated first by wave forcing (surfzone and shallow inner shelf), then cross-shelf wind forcing (inner shelf), and then along-shelf wind forcing (midshelf; Fig. 15).

The cross-shelf circulation driven by cross-shelf winds on the inner shelf, and its dependence on season and presumably on stratification, is substantial. These cross-shelf flows have important implications for the transport of nutrients, larvae, pollutants, heat, and salt on inner continental shelves. When considering transport of nutrients and other tracers, we must consider Lagrangian particle trajectories, on which waves have a strong effect at this site. The estimated Lagrangian cross-shelf velocity profile in winter resembles just the wind-driven part of the Eulerian velocity profile. When the Stokes drift profile is added to the Eulerian velocity profile to form the Lagrangian profile estimate, the Stokes drift tends to cancel the wave-driven part of the Eulerian velocity profile, leaving only the wind-driven part.

The MVCO site is typical of many shallow coastal

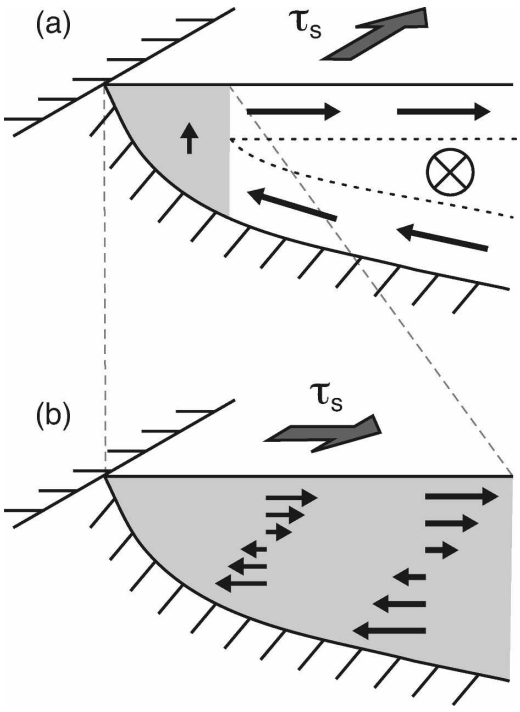

FIG. 14. Cross-shelf circulation driven by a steady along-shelf or cross-shelf wind stress, assuming along-shelf uniform flow. (a) Cross-shelf circulation (black arrows) driven by an upwelling-favorable wind stress $\boldsymbol{\tau}_s$ (gray arrow). At midshelf (on the right-hand side of the upper diagram) the cross-shelf flow is offshore in the surface boundary layer, with a return flow in the bottom boundary layer (as shown) or in the interior; the along-shelf flow is in the direction of the wind stress (circle with x). Over the inner shelf (light gray shading) where the surface and bottom boundary layers (dashed lines) overlap, the cross-shelf flow is weak compared to midshelf, and upwelling occurs. (b) Cross-shelf circulation (black arrows) driven by an offshore wind stress $\boldsymbol{\tau}_s$ (gray arrow) over the inner shelf. The inner shelf (light gray shading) extends over the entire region shown, which is the same region as the shaded region in (a). Due to the overlapping surface and bottom boundary layers, the cross-shelf circulation near the surface is in the direction of the wind stress, with a return flow lower in the water column.

Unauthenticated | Downloaded 10/26/25 08:20 PM UTC

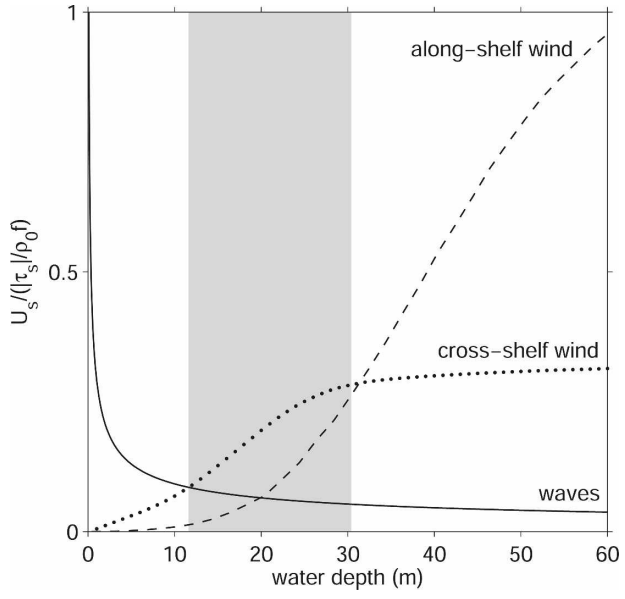

FIG. 15. Relative importance of cross-shelf wind stress, along-shelf wind stress, and wave forcing: theoretical cross-shelf surface layer transport U_s normalized by deep-water Ekman transport $|\boldsymbol{\tau}_s|/\rho_0 f$, as a function of water depth. The U_s is calculated numerically for cross-shelf or along-shelf wind based on a model with constant density, wind stress magnitude 0.1 Pa, and a bilinear cutoff eddy viscosity profile (Lentz 1995). The U_s is estimated for wave forcing via $U_s = gH_{\text{sig}}^2/16c$, using the shallow-water phase speed $c = \sqrt{gh}$ and the relation $H_{\text{sig}}^2 \sim (15\ \text{m}^2\ \text{Pa}^{-1})|\boldsymbol{\tau}_s|$ observed at MVCO. The region where cross-shelf wind stress is the dominant forcing mechanism is shaded gray. This is a conservative estimate; a cubic eddy viscosity profile predicts a wider region.

sites. The strength of the wind stress at MVCO is not unusual compared to other midlatitude sites. The dependence that we describe for MVCO of the cross-shelf velocity profile on the cross-shelf wind should apply to many unsheltered inner shelf locations.

Acknowledgments. This manuscript was greatly improved due to suggestions by John Trowbridge. Ken Brink, Robert Beardsley, Heidi Sosik, J. Tom Farrar, Carlos Moffat-Varas, Glenn Flierl, and two anonymous reviewers also provided very helpful and detailed comments. Robert Beardsley and Carlos Moffat-Varas provided a MATLAB version of the COARE bulk algorithms. This research was funded by the Ocean Sciences Division of the National Science Foundation under Grants OCE-0241292 and OCE-0548961 and by National Aeronautics and Space Administration Headquarters under Grant NNG04GL03G and the Earth System Science Fellowship Grant NNG04GQ14H. MVCO is partly funded by the Woods Hole Oceanographic Institution and the Jewett/EDUC/Harrison Foundation.

REFERENCES

Allen, J. S., 1980: Models of wind-driven currents on the continental shelf. *Annu. Rev. Fluid Mech.,* **12,** 389–433.

Andrews, D. G., and M. E. McIntyre, 1976: Planetary waves in horizontal and vertical shear: The generalized Eliassen–Palm relation and the mean zonal acceleration. *J. Atmos. Sci.,* **33,** 2031–2048.

Austin, J. A, 1999: The role of the alongshore wind stress in the heat budget of the North Carolina inner shelf. *J. Geophys. Res.,* **104,** 18 187–18 204.

——, and S. J. Lentz, 1999: The relationship between synoptic weather systems and meteorological forcing on the North Carolina inner shelf. *J. Geophys. Res.,* **104,** 18 159–18 185.

——, and ——, 2002: The inner shelf response to wind-driven upwelling and downwelling. *J. Phys. Oceanogr.,* **32,** 2171–2193.

Beardsley, R. C., D. C. Chapman, K. H. Brink, S. R. Ramp, and R. Schlitz, 1985: The Nantucket Shoals Flux Experiment (NSFE79). Part I: A basic description of the current and temperature variability. *J. Phys. Oceanogr.,* **15,** 713–748.

Berger, T. J., W. C. Boicourt, J. H. Churchill, P. Hamilton, R. J. Wayland, and D. R. Watts, 1994: A physical oceanographic field program offshore of North Carolina. Science Applications International Corporation Tech. Rep. MMS 94, 463 pp.

Biscaye, P. E., C. N. Flagg, and P. G. Falkowski, 1994: The Shelf Edge Exchange Processes experiments, SEEP-II: An introduction to hypotheses, results and conclusions. *Deep-Sea Res. II,* **41,** 231–252.

Blanton, J. O., 1981: Ocean currents along a nearshore frontal zone on the continental shelf of the southeastern United States. *J. Phys. Oceanogr.,* **11,** 1627–1637.

Brink, K. H., 1998: Wind-driven currents over the continental shelf. *The Global Coastal Ocean: Processes and Methods,* K. H. Brink and A. R. Robinson, Eds.,Vol. 10, *The Sea: Ideas and Observations on Progress in the Study of the Seas,* Wiley & Sons, 3–20.

Brown, W. S., J. D. Irish, and C. D. Winant, 1987: A description of subtidal pressure field observations on the northern California continental shelf during the Coastal Ocean Dynamics Experiment. *J. Geophys. Res.,* **92,** 1605–1636.

——, N. R. Pettigrew, and J. D. Irish, 1985: The Nantucket Shoals Flux Experiment (NSFE79). Part II: The structure and variability of across-shelf pressure gradients. *J. Phys. Oceanogr.,* **15,** 749–771.

Csanady, G. T., 1978: The arrested topographic wave. *J. Phys. Oceanogr.,* **8,** 47–62.

Cudaback, C. N., L. Washburn, and E. Dever, 2005: Subtidal inner-shelf circulation near Point Conception, California. *J. Geophys. Res.,* **110,** C10007, doi:10.1029/2004JC002608.

Ekman, V. W., 1905: On the influence of the Earth's rotation on ocean-currents. *Arkiv Matematik, Astron. Fysik,* **2,** 1–53.

Falkowski, P. G., R. T. Barber, and V. Smetacek, 1998: Biogeochemical controls and feedbacks on ocean primary production. *Science,* **281,** 200–206.

Fewings, M. R., 2007: Cross-shelf circulation and momentum and heat balances over the inner continental shelf near Martha's Vineyard, Massachusetts. Ph.D. thesis, Woods Hole Oceanographic Institution/Massachussetts Institute of Technology Joint Program in Oceanography/Applied Ocean Science and Engineering, 267 pp. [Available online at http://hdl.handle.net/1912/2121.]

Fratantoni, P. S., and R. S. Pickart, 2003: Variability of the shelf

Unauthenticated | Downloaded 10/26/25 08:20 PM UTC

break jet in the Middle Atlantic Bight: Internally or externally forced? *J. Geophys. Res.,* **108,** 3166, doi:10.1029/2002JC001326.

Garvine, R. W., 1971: A simple model of coastal upwelling dynamics. *J. Phys. Oceanogr.,* **1,** 169–179.

Hasselmann, K., 1970: Wave-driven inertial oscillations. *Geophys. Fluid Dyn.,* **1,** 463–502.

Hutto, L., T. Farrar, and R. A. Weller, 2005: CBLAST 2003 field work report. Woods Hole Oceanographic Institution Tech. Rep. WHOI-2005-04, 136 pp.

Huyer, A., 1983: Coastal upwelling in the California Current system. *Prog. Oceanogr.,* **12,** 259–284.

Kirincich, A. R., J. A. Barth, B. A. Grantham, B. A. Menge, and J. Lubchenco, 2005: Wind-driven inner-shelf circulation off central Oregon during summer. *J. Geophys. Res.,* **110,** C10S03, doi:10.1029/2004JC002611.

Lee, T. N., W. J. Ho, V. Kourafalou, and J. D. Wang, 1984: Circulation on the continental shelf of the southeastern United States. Part I: Subtidal response to wind and Gulf Stream forcing during winter. *J. Phys. Oceanogr.,* **14,** 1001–1012.

——, E. Williams, R. E. J. Wang, and L. Atkinson, 1989: Response of South Carolina continental shelf waters to wind and Gulf Stream forcing during winter of 1986. *J. Geophys. Res.,* **94,** 10 715–10 754.

Lentz, S. J., 1994: Current dynamics over the northern California inner shelf. *J. Phys. Oceanogr.,* **24,** 2461–2478.

——, 1995: Sensitivity of the inner-shelf circulation to the form of the eddy viscosity profile. *J. Phys. Oceanogr.,* **25,** 19–28.

——, 2001: The influence of stratification on the wind-driven cross-shelf circulation over the North Carolina shelf. *J. Phys. Oceanogr.,* **31,** 2749–2760.

——, 2008: Observations and a model of the mean circulation over the Middle Atlantic Bight continental shelf. *J. Phys. Oceanogr.,* **38,** 1203–1221.

——, R. T. Guza, S. Elgar, F. Feddersen, and T. H. C. Herbers, 1999: Momentum balances on the North Carolina inner shelf. *J. Geophys. Res.,* **104,** 18 205–18 226.

——, M. R. Fewings, P. Howd, J. Fredericks, and K. Hathaway, 2008: Observations and a model of undertow over the inner continental shelf. *J. Phys. Oceanogr.,* 2341–2357.

Li, Z., and R. H. Weisberg, 1999a: West Florida continental shelf response to upwelling favorable wind forcing 2. Dynamics. *J. Geophys. Res.,* **104,** 23 427–23 442.

——, and ——, 1999b: West Florida shelf response to upwelling favorable wind forcing: Kinematics. *J. Geophys. Res.,* **104,** 13 507–13 527.

Linder, C. A., and G. Gawarkiewicz, 1998: A climatology of the shelfbreak front in the Middle Atlantic Bight. *J. Geophys.* **103,** 18 405–18 423.

Liu, Y., and R. H. Weisberg, 2005: Momentum balance diagnoses for the West Florida Shelf. *Cont. Shelf Res.,* **25,** 2054–2074.

Longuet-Higgins, M. S., 1953: Mass transport in water waves. *Philos. Trans. Roy. Soc. London,* **A245,** 535–581.

McCreary, J. P., H. S. Lee, and D. B. Enfield, 1989: The response of the coastal ocean to strong offshore winds: With application to circulations in the Gulfs of Tehuantepec and Papagayo. *J. Mar. Res.,* **47,** 81–109.

Noble, M., and B. Butman, 1983: On the longshelf structure and dynamics of subtidal currents on the eastern United States Continental Shelf. *J. Phys. Oceanogr.,* **13,** 2125–2146.

Pawlowicz, R., R. C. Beardsley, and S. J. Lentz, 2002: Harmonic analysis including error estimates in MATLAB using T_TIDE. *Comput. Geosci.,* **28,** 929–937.

Roughgarden, J., S. Gaines, and H. Possingham, 1988: Recruitment dynamics in complex life cycles. *Science,* **241,** 1460–1466.

Schofield, O., T. Bergmann, P. Bissett, J. F. Grassle, D. B. Haidvogel, J. Kohut, M. Moline, and S. M. Glenn, 2002: The long-term ecosystem observatory: An integrated coastal observatory. *IEEE J. Oceanic Eng.,* **27,** 146–154.

Shearman, K., and S. J. Lentz, 2003: Dynamics of mean and subtidal flow on the New England shelf. *J. Geophys. Res.,* **108,** 3218, doi:10.1029/2002JC001417.

——, and ——, 2004: Observations of tidal variability on the New England shelf. *J. Geophys. Res.,* **109,** C06010, doi:10.1029/2003JC001972.

Smith, R. L., 1981: A comparison of the structure and variability of the flow field in three coastal upwelling regions: Oregon, Northwest Africa, and Peru. *Coastal Upwelling,* F. A. Richards, Ed., Amer. Geophys. Union, 107–118.

Smith, S. D., 1988: Coefficients for sea surface wind stress, heat flux, and wind profiles as a function of wind speed and temperature. *J. Geophys. Res.,* **93,** 15 467–15 472.

Stokes, G. G., 1847: On the theory of oscillatory waves. *Trans. Cambridge Philos. Soc.,* **8,** 441–455.

Sverdrup, H. U., 1938: On the process of upwelling. *J. Mar. Res.,* **1,** 155–164.

Thompson, K. R., and D. T. Pugh, 1986: The subtidal behavior of the Celtic Sea—II. Currents. *Cont. Shelf Res.,* **5,** 321–346.

Tilburg, C. E., 2003: Across-shelf transport on a continental shelf: Do across-shelf winds matter? *J. Phys. Oceanogr.,* **33,** 2675–2688.

Walsh, J. J., P. E. Biscaye, and G. T. Csanady, 1988: The 1983–1984 Shelf Edge Exchange Processes (SEEP)-I experiment: Hypotheses and highlights. *Cont. Shelf Res.,* **8,** 435–456.

Weatherly, G. L., and P. J. Martin, 1978: On the structure and dynamics of the oceanic bottom boundary layer. *J. Phys. Oceanogr.,* **8,** 557–570.

Xu, Z., and A. J. Bowen, 1994: Wave- and wind-driven flow in water of finite depth. *J. Phys. Oceanogr.,* **24,** 1850–1866.

Unauthenticated | Downloaded 10/26/25 08:20 PM UTC